

TIMING AND SCINTILLATIONS OF THE MILLISECOND PULSAR 1937+214

J. M. CORDES

Astronomy Department and National Astronomy and Ionosphere Center, Cornell University

A. WOLSZCZAN

National Astronomy and Ionosphere Center, Cornell University

R. J. DEWEY

Center for Radiophysics and Space Research, Cornell University

M. BLASKIEWICZ

Department of Physics and NAIC, Cornell University

AND

D. R. STINEBRING

Department of Physics, Princeton University

Received 1989 March 13; accepted 1989 July 17

ABSTRACT

Pulse shapes, arrival times, and interstellar scintillations of the 1.56 ms pulsar are analyzed at frequencies from 0.32 to 1.4 GHz using data obtained from 1983 April to 1985 December. The two pulse components (main pulse and interpulse) are different in shape, and their separation is weakly frequency dependent, decreasing from $173^{\circ}6$ to $173^{\circ}0$ of pulse phase between 0.43 and 1.4 GHz. Pulse shapes at the lowest frequencies show broadening caused by scattering in the interstellar medium that is consistent with the intensity scintillations that are also seen. The occurrence of fast scintillations of the pulsar intensity demonstrates that the broadening is caused by multipath scattering rather than by angular wandering of a single ray path.

We test the precision to which the measured pulse phase represents the true rotational phase of the pulsar. Intrinsic phase jitter of individual pulses ($\sim 15 \mu\text{s}$) causes time of arrival errors in sums of N pulses that scale roughly as $N^{-1/2}$. At low frequencies, the largest time of arrival errors are due to interstellar scintillations. Scintillation-induced frequency structure changes on time scales ~ 1 minute, introducing arrival time errors of a few microseconds. On time scales of months and longer, the measured pulse phase varies in a wavelength-dependent manner.

The long-term, wavelength-dependent time of arrival variations, if interpreted as dispersion measure changes, are $\delta\text{DM} \approx 0.003 \text{ pc cm}^{-3}$ over 1000 days. However, it is unclear whether the wavelength dependent variations are due *solely* to DM variations. At two epochs, the variations at three frequencies show the ν^2 scaling expected from dispersion measure variations. However, comparison of DMs calculated from 1.4 to 2.4 GHz data (published by Rawley *et al.* in 1988) with those calculated from 0.43–1.4 GHz data are inconsistent: the first set is systematically larger than the second set of DMs. The bias may indicate that (1) arrival times are perturbed by changes in pulse shape with frequency; (2) there are additional contributions from interstellar scattering, including angle of arrival effects that contribute $\sim \nu^2$ and $\sim \nu^4$ perturbations to arrival times; (3) the volume of interstellar scattering material that is sampled is a function of frequency, owing to the scaling of the scattering diameter $\propto \nu^{2.2}$; and (4) there is nonsimultaneous emission of different frequencies toward Earth due to a variation in altitude of emission combined with rotational aberration, reference frame dragging, gravitational bending of rays, and magnetic field line distortion. Further exploration of these possibilities will require additional measurements at many frequencies between 0.3 and 3 GHz.

Time series of scintillation parameters are consistent with scattering in the interstellar medium from electron density irregularities with a spectrum (wavenumber) $^{-\alpha}$ with $\alpha = 3.55 \pm 0.11$. The Kolmogorov spectrum ($\alpha = 11/3$) is consistent with these results. The range of length scales encompassed by the spectrum is at least 10^{11} – 10^{14} cm with the lower limit probably extending down to 10^9 cm or less. The distribution of scattering material along the line of sight appears to be nearly uniform. Refraction from large-scale irregularities in the ISM evidently produces angular wandering of the pulsar image that is much less than the diffractive broadening of the image.

Subject headings: interstellar: matter — pulsars — stars: individual (PSR 1937+214)

I. INTRODUCTION

Of the known pulsars, the millisecond pulsar 1937+214 is the most rotationally stable (Davis *et al.* 1985; Rawley *et al.* 1987; Rawley, Taylor, and Davis 1988), evidently because its small spindown rate induces little dynamical noise in the internal torques of the neutron star (Cordes and Downs 1985;

Alpar, Nandkumar, and Pines 1986). In addition, the narrow pulse and short period allow times of arrival (TOAs) to be determined more precisely by one or two orders of magnitude than TOAs of other pulsars. These increases in TOA precision and rotational stability allow measurement of propagation time variations due to uncertainties in the location of Earth,

changes in metric, and plasma propagation effects along the line of sight (Cordes and Stinebring 1984; Blandford, Narayan, and Romani 1984; Davis *et al.* 1985; Rawley *et al.* 1987; Rawley, Taylor, and Davis 1988).

In this paper, we discuss a combined arrival time, pulse shape, and scintillation study based on data obtained at the Arecibo Observatory. It is well known that interstellar scattering can cause time-variable pulse-shape distortion and arrival time fluctuations (Armstrong 1984; Blandford, Narayan, and Romani 1984; Cordes, Pidwerbetsky, and Lovelace 1986, hereafter CPL). However, uncertainties in the nature of electron density variations prohibit detailed predictions of the arrival time fluctuations. One of our aims, therefore, was to use scintillation and timing observations to constrain the electron density wavenumber spectrum. As a consequence, our choice of observing frequencies was made so as to maximize scattering effects and is therefore complementary to frequencies used by Rawley *et al.* (1987), who hoped to minimize scattering effects by observing at high frequency.

In § II we summarize the observations and preliminary analysis. Short-term (intraday) timing and scintillation variations are discussed in § III, where we analyze intrinsic pulse phase jitter (probably a pulsar magnetospheric effect), pulse shape variations induced by interstellar scintillations, and their relationship to time of arrival estimates. Long-term variations are presented in § IV. Constraints on the electron density wavenumber spectrum are made in § V. Our conclusions are summarized in § VI.

II. OBSERVATIONS

Observations were made at the Arecibo Observatory from 1983 April through 1985 December using the 305 m reflector and line feed antennas at 0.32, 0.43, 0.60, 0.93, and 1.4 GHz. A preliminary analysis of the 1983 April data has been reported by Cordes and Stinebring (1984), where the data acquisition is described and a precise value of the dispersion measure is given. Polarization results have been reported by Stinebring and Cordes (1983).

We recorded the predetection signal that is proportional to the electric field accepted by the feed antenna and heterodyned to zero frequency ("base band") by a series of local oscillators. The base band voltage may be considered complex because in-phase and quadrature components are needed to fully characterize it. Complex samples were obtained at the Nyquist rate appropriate for the bandwidth imposed on the signal. Bandwidths of 125 kHz were used at 0.32 and 0.43 GHz, while 250 kHz filters were used at 0.43, 0.60, 0.93, and 1.4 GHz. Some 1.4 GHz data were obtained with 500 kHz bandwidths (using a single polarization channel) to study the pulse waveform with the highest resolution. Late in 1984, we realized that low-level features in the baseline of 0.43 GHz waveforms (cf. Stinebring *et al.* 1984) resulted from aliasing of strong scintillation features in the sidelobes of the bandpass filter. To suppress aliasing, we reduced the bandwidth to 125 kHz and sampled at twice the Nyquist rate. The Nyquist sample intervals were 1.9, 3.9, and 7.9 μ s when using bandwidths of 500, 250, and 125 kHz. The true resolution for frequencies below 1 GHz is determined by interstellar scattering, which causes pulse broadening that scales roughly as $\tau_{\text{iss}} \approx 0.61\nu^{-4.4}$ μ s, where ν is the frequency in GHz (see analysis below).

Data were usually written to magnetic tape directly, although our earlier work (Cordes and Stinebring 1984) involved real time dispersion removal. Off-line analysis caused by interstellar scattering is evident. Waveforms at 0.43

sisted of (1) formation of pulse waveforms after removal of interstellar dispersion distortion and (2) computation of the intensity as a function of time and radio frequency (the dynamic spectrum), useful for studying interstellar scintillations.

Dispersion removal was accomplished using the digital filtering technique developed by Hankins (1971; see also Hankins and Rickett 1975), which corrects the Fourier phases of the base-band signal and requires knowledge of the dispersion measure to an accuracy of 0.2% or better (cf. Fig. 1 of Cordes and Stinebring 1984). This predetection technique is superior to postdetection dispersion removal (e.g., Taylor and Huguenin 1971; Boriakoff 1973) for time of arrival studies because the dispersion induced phase is corrected across the entire bandpass. The resultant arrival times are insensitive to the precise frequencies of scintillation-induced intensity maxima, which vary on time scales of minutes.

After dispersion removal, the resultant pulse trains were averaged synchronously to form pulse waveforms. These waveforms were subjected to further analysis that included (1) template fitting to obtain arrival times and (2) a shape analysis to determine the temporal broadening time. We studied these quantities using averages of 240 pulses (the minimum needed to get a usable signal to noise ratio) to 2×10^5 pulses (the maximum obtained in an observing session) on a given day. We also analyzed timing and scintillations over the course of the 2.8 yr time span of our entire data set.

Grand average waveforms are shown in Figure 1. Table 1 gives waveform parameters, including the widths and separation of the main pulse and interpulse. The 1.4 GHz pulse is sharpest and the main pulse, the larger of the two components separated by $\sim 173^\circ$ (where pulse phase is measured in degrees), shows an additional feature separated by $\sim 8:1$ of ~ 35 μ s from the maximum. This structure is presumably related to the double pulse structure seen from many pulsars (Rankin 1983; Lyne and Manchester 1988). The main pulse-to-interpulse amplitude ratio ($\sim 45\%$) is not strongly frequency-dependent, and the separation is weakly frequency-dependent. At 0.43 and 0.32 GHz, the asymmetry of the pulses

TABLE 1
WAVEFORM PARAMETERS

Frequency (GHz)	Main Pulse Width (FWHM) (μ s)	Interpulse Width (FWHM) (μ s)	Separation
0.32 ^a	111 (45) ^b	161 (45)	173.2 \pm 0.3
0.43	61 (45)	68 (45)	173.56 \pm 0.03
0.61 ^a	56 (43)	59 (44)	172.2 \pm 0.2
1.40	40 ^d	49	173.01 \pm 0.04
2.38 ^c	43	47	173 \pm 1

^a Data obtained in a single linear polarization. Waveform data are probably biased by the strong polarization of the pulsar signal.

^b Values in parentheses derive from a least-squares fit of a Gaussian function convolved with a one-sided exponential, as discussed in text.

^c The separation of main and interpulse was found by fitting a template to the main pulse and interpulse separately for a large number of individual waveforms. Errors (± 1 standard deviation) on the mean are given.

^d Width excludes the secondary main pulse feature that is about 35 μ s after the maximum (cf. Fig. 1).

^e Results from Stinebring 1983 and Rawley 1986.

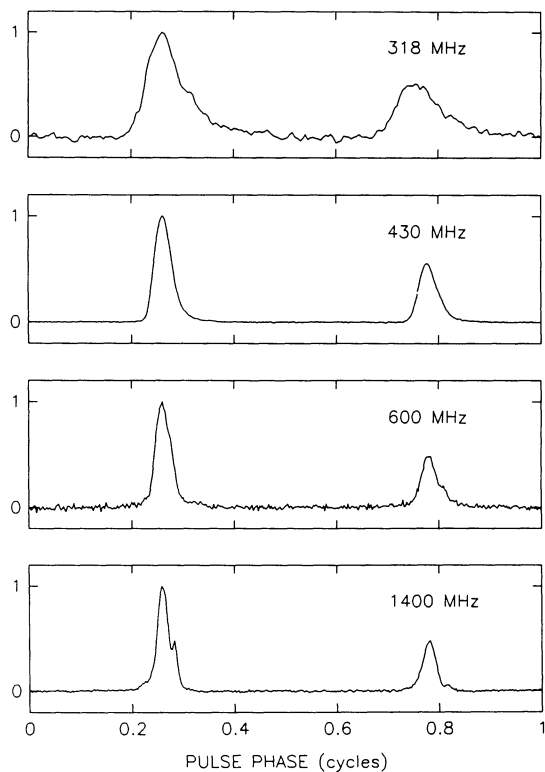


FIG. 1.—Waveforms at 1.4, 0.6, 0.43, and 0.32 GHz

and 1.4 GHz are total intensities, whereas the others represent only one sense of linear polarization. The linearly polarized waveforms are distorted by time-variable Faraday rotation and rotation of the feed antenna as the source is tracked. For this reason we concentrate on the 0.43 and 1.4 GHz data in the arrival time analysis discussed below.

Scintillations were studied through the computation of dynamic spectra. These were computed from the base-band voltage by Fourier transforming raw records, squaring, and averaging spectra for 8 s (100 records). Spectra were truncated at the edges and fitted with a third-order polynomial to remove the bandpass filter shape. For a few subsets of data (such as are shown in Fig. 5), we used an alternative analysis that gave greater signal-to-noise ratio in the scintillation spectra: we computed dynamic spectra *after* dispersion removal by finding the spectrum when the pulse was “ON” and differencing and normalizing by a similar “OFF” pulse spectrum. Dynamic spectra were used to quantify the scintillations at each epoch, as discussed below.

In the following we discuss the observables on both short (intraday) and long time scales.

III. SHORT TIME SCALE INTENSITY AND TIMING VARIATIONS

a) Time of Arrival Variations

Arrival times were estimated in standard ways (e.g., Helfand *et al.* 1980) by cross-correlating a high signal-to-noise ratio waveform from 1.4 GHz with all other waveforms. The lag of maximum correlation is combined with the time of the first sample in each data record to yield the topocentric arrival time. The time tagging of the first sample has a nominal accuracy of $1 \mu\text{s}$ (discussed further in § IVc). Figure 2 shows examples of cross-correlation functions and the fitted parabolas

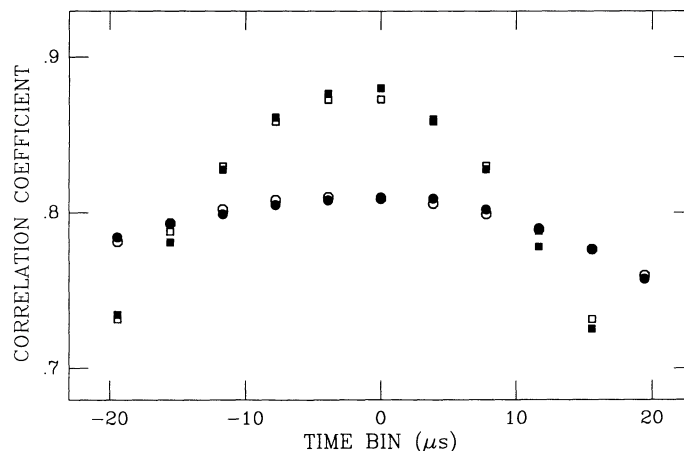


FIG. 2.—Results of template fitting to trial waveforms. Cross-correlation function between the template and a 1.4 GHz waveform (*squares*) and a 0.43 GHz waveform (*circles*). Filled symbols represent the data; open symbols, a fitted parabola.

used to find the maxima. Formal errors of template fits are typically only $0.2 \mu\text{s}$, far smaller than the observed time of arrival variations on time scales of minutes. The true errors are determined by interstellar scintillations and by the sampling of the data.

Figure 3 shows autocorrelation functions of short-term TOA variations at 0.43 and 1.4 GHz. The rms TOA variation is $2.2 \mu\text{s}$ at 0.43 GHz and $0.7 \mu\text{s}$ at 1.4 GHz for the particular data sets shown. At 0.43 GHz the TOA variations are correlated over about 80 s (the approximate lag of zero crossing). This time scale is nearly the same as the characteristic time scale of interstellar scintillations at this frequency (see the discussion below in § IIc). By contrast, the 1.4 GHz TOA variations are consistent with white noise, as shown by the spike in the autocorrelation function that decays to almost zero at a lag of one sample. As we discuss in detail in § IIc, this difference in

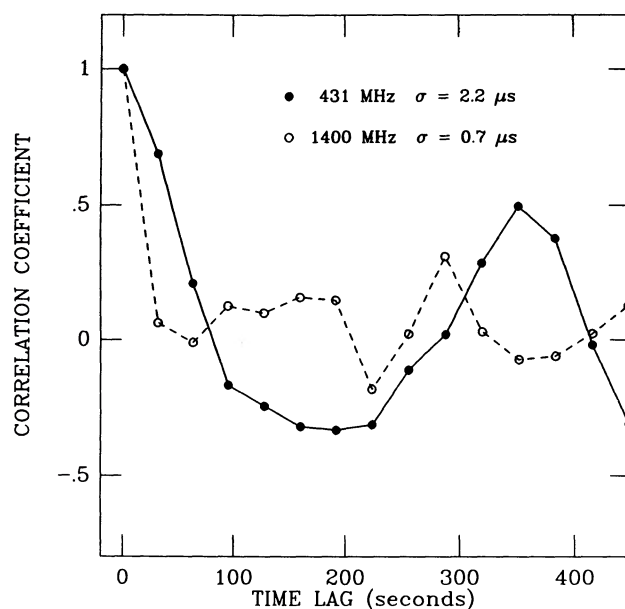


FIG. 3.—Autocorrelation functions of the times of arrival computed from a series of 32 s average waveforms.

behavior arises because at 0.43 GHz arrival time perturbations are scintillation-dominated, while at 1.4 GHz they are dominated by radiometer noise and phase jitter intrinsic to the pulsar.

b) Intrinsic Pulse Phase Jitter

We have used our 1.4 GHz data to estimate the amount by which individual pulses move randomly in pulse phase with respect to a fiducial phase locked to the rotational phase of the pulsar. Jitter is necessarily intrinsic to the pulsar because interstellar (as well as interplanetary and ionospheric) propagation effects occur on much longer time scales. All well-studied pulsars show intrinsic phase variations on pulse-to-pulse time scales (Taylor and Huguenin 1971; Backer 1973; Helfand, Manchester, and Taylor 1975; Downs and Krause-Polstorff 1986) that are usually assumed to be distinct from the "red" timing noise that is manifest on much longer time scales (Boynton *et al.* 1972; Cordes and Helfand 1980; Cordes and Downs 1985; Alpar, Nandkumar, and Pines 1986). In some cases the short-term phase variations appear as semirepetitive drifts ("drifting subpulses"), while in others phase variations are statistically independent between contiguous pulse periods. The distinction between phase jitter and longer term timing noise is as follows: jitter occurs with respect to a well-defined fiducial phase that is tied to a point on the neutron star surface. Physically, jitter is probably associated with motions of emission regions with respect to a magnetic pole. Timing noise, on the other hand, represents actual departures in the rotational phase from that expected for an object that is smoothly spinning down.

We have investigated 1.4 GHz TOA variations during a strong scintillation maximum when the signal-to-noise ratio was large. We formed a set of 480 pulse waveforms, each of which was an average of 240 single pulses. TOAs were found for each and for sums of these basic waveforms. We thereby obtained TOAs for averages of N pulses with N ranging from 240 to 7680 pulses.

Results are shown in Figure 4, where the rms TOA is plotted as a function of N for the main pulse (MP) and interpulse (IP) components separately. For both components, the rms TOA decreases roughly as $N^{-1/2}$ for $N \leq 1000$, as would be expected for errors due to additive system noise and intrinsic pulse jitter. For larger N , the rms TOA for the main pulse flattens, while that for the interpulse continues to decrease. This difference may signify a real difference in the fluctuation properties of the two pulse components. Alternatively, it may arise from binning effects in TOA estimation that depend on the signal to noise ratio, such as those suggested by Rawley (1986). These binning effects arise (J. Taylor, private communication) from the template-fitting procedure when the TOA precision becomes much smaller than one sample interval. In this regime, the precision ceases to decline as N gets larger and the signal-to-noise ratio gets larger. Clearly, for a given N , this regime happens to the main pulse before the interpulse. In any case, our data set is too short to probe the large N behavior of the rms TOA in more detail. Our main concern here is to extrapolate to $N = 1$ from the small N portions of the curves in Figure 4, which satisfy the understandable $N^{-1/2}$ scaling.

We model variations in TOA for an N -pulse average as a sum of two terms, one involving the signal-to-noise ratio $\sigma_{\text{SNR}}(N)$, and the other representing intrinsic pulse phase

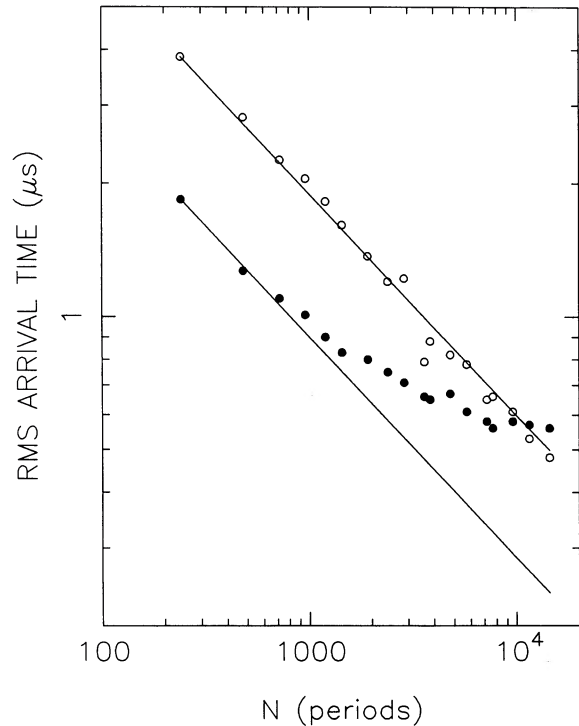


FIG. 4.—Root mean square time of arrival computed from averages of different numbers of pulses. Curves are shown separately for the main pulse (filled circles) and interpulse (open circles). Solid lines show variations $\propto N^{-1/2}$ expected from a combination of random noise and random pulse jitter.

jitter $\sigma_j(N)$:

$$\sigma(N) = [\sigma_j^2(N) + \sigma_{\text{SNR}}^2(N)]^{1/2}. \quad (1)$$

Because the second term in the TOA variance is signal-to-noise-dependent, it is possible to separate the two contributions if we assume that jitter is intensity-independent. This assumption may not be warranted since, for example, Krishnamohan and Downs (1983) found that short-term pulse phase variations are correlated with intensity for the Vela pulsar. However, it is not known if other pulsars behave in the same way, and, for our analysis, we seek only a crude estimate of the jitter amplitude.

To estimate σ_j , we assume that it is the same for both the mainpulse and interpulse. This assumption appears reasonable, since longer period pulsars show phase jitter that is roughly some fixed fraction of the integrated pulse width; σ_{SNR} depends on the signal to noise ratio as (Downs and Reichley 1983)

$$\sigma_{\text{SNR}} \propto [\text{SNR}(N)\sqrt{N}]^{-1}.$$

By estimating rms TOAs $\sigma_{\text{mp}}(N)$, $\sigma_{\text{ip}}(N)$ and signal-to-noise ratios $\text{SNR}_{\text{mp}}(N)$ and $\text{SNR}_{\text{ip}}(N)$ as a function of N , we may solve for the rms jitter as

$$\sigma_j^2(N) = \frac{r^2 \sigma_{\text{mp}}^2(N) - \sigma_{\text{ip}}^2(N)}{r^2 - 1}, \quad (2)$$

where $r \equiv \text{SNR}_{\text{mp}}/\text{SNR}_{\text{ip}} = 2.25 \pm 0.05$ is the ratio of SNRs found using all the 1984 and 1985 data. By using the numbers in Figure 4 for $N = 240$ and extrapolating to $N = 1$, we find that $\sigma_j(1) = 15 \pm 10 \mu\text{s}$. The phase jitter may be compared to

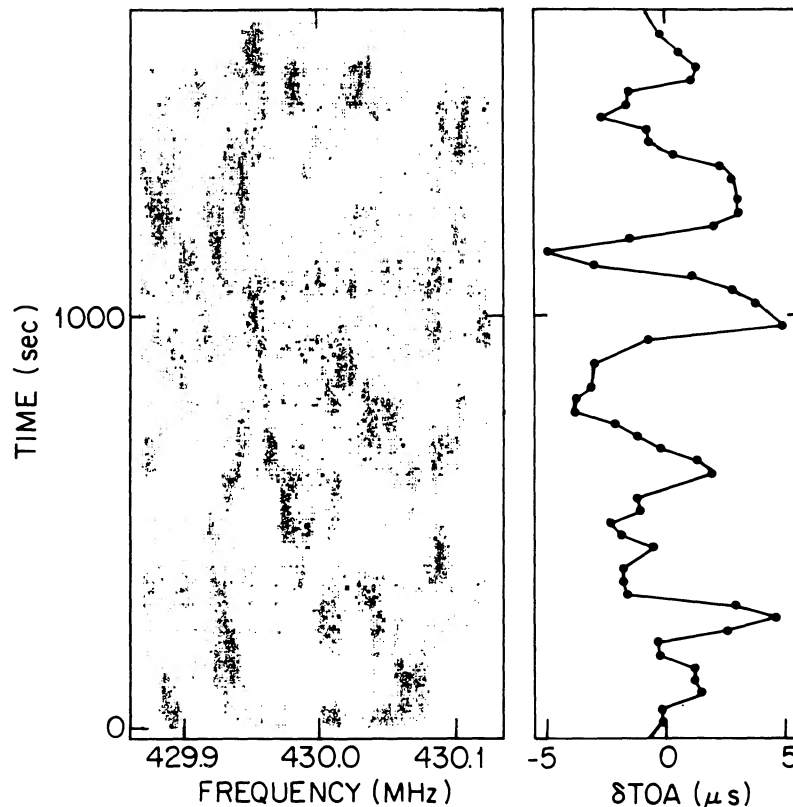


FIG. 5.—Comparison of interstellar scintillations and short-term time of arrival variations. *Left panel:* Dynamic spectra at 430 MHz. The gray scale is linear, with the blackest corresponding to higher intensity and white corresponding to intensities less than 50% of the maximum. *Right panel:* Deviation from the mean of the time of arrival determined from 32 s average waveforms.

the widths (FWHM) of about $40 \mu\text{s}$ and $45 \mu\text{s}$ for both the main pulse and interpulse, respectively (Table 1).

c) Interstellar Scintillations and Temporal Broadening

In this section we demonstrate that the precision of arrival times at 0.43 GHz is limited by the frequency structure in the pulsar signal imposed by multipath propagation through the ISM. The notation we use is as follows: in quantifying scintillations, $\Delta\nu_d$ and Δt_d denote the scintillation frequency and time scales. These are the characteristic bandwidth and time over which the intensity is correlated, owing to diffractive scattering. The quantity τ_d is the pulse-broadening time which satisfies the “uncertainty” relation, $2\pi\tau_d\Delta\nu_d \approx 1$.

Figure 5 shows interstellar scintillations in the form of dynamic spectra along with arrival times determined from averages of 2400 pulses for the same data at 0.43 GHz. The gray scale plot of the scintillations shows the usual bands of constructive and destructive interference that arise from multipath propagation. The bands have characteristic widths in time and frequency that are the scintillation or diffraction bandwidth $\Delta\nu_d$ and time scale Δt_d . The appearance of scintillation frequency structure is direct proof that diffractive multipath scattering occurs.

The arrival times in Figure 5 vary by about $\pm 5 \mu\text{s}$, about 20 times larger than the formal errors expected in the template-fitting process described above. The frequency structure in the pulsar signal introduced by interstellar scintillations can cause TOA errors by two distinct effects: (1) a change $\delta\nu$ in the effective center frequency of the signal, resulting in a TOA

change $\delta t \propto DM\delta\nu$; and (2) a change in the net pulse shape caused by the detailed shapes of the intensity maxima that are instantaneously in the receiver bandpass. The first effect is eliminated by proper removal of dispersion delays across the receiver bandpass, as we have done in this paper. The second effect causes the $\pm 5 \mu\text{s}$ TOA variations seen in Figure 5. To the eye there is no obvious relation between the TOA variations and the scintillation variations in the figure. This is because the TOA variations are associated with the *widths* (in frequency) of scintillation features in the spectrum. The second effect can be minimized only by making observations that include as many scintillation maxima as possible before calculation of arrival times. In principle, the TOAs could be corrected by using the information contained in the spectra. We have made initial attempts at this, but the signal-to-noise ratio in our data appears inadequate for achieving significant improvement.

The notable feature of the scintillations in Figure 5 is that the number of bright features (N_{iss}) in the two-dimensional (time and frequency) frame is small. For a receiver bandwidth $\Delta\nu$ and integration time T , the number of such features is

$$N_{\text{iss}} \approx \left(1 + \zeta \frac{\Delta\nu}{\Delta\nu_d}\right) \left(1 + \zeta \frac{T}{\Delta t_d}\right), \quad (3)$$

where $\zeta \approx 0.1\text{--}0.2$ is an empirically determined coefficient. (In the limit of large $\Delta\nu/\Delta\nu_d$ and $T/\Delta t_d$ this is the same as eq. [7] in Cordes 1986).

TOA fluctuations arise because the net observed pulse shape is the convolution of the intrinsic pulse shape with a function that depends on the characteristic bandwidth of the scintil-

lations (see Appendix). As is well known (e.g., Rickett 1977), in the limit of an ensemble average, the observed pulse shape is the convolution of the intrinsic pulse shape with a one-sided exponential function if scintillations result from scattering by a thin screen. The $1/e$ broadening time is $\tau_d = (2\pi\Delta\nu_d)^{-1}$. Thicker media yield exponential like functions with a finite rise time (e.g., Williamson 1972, 1975). For finite averages over N_{iss} independent scintillation fluctuations, however, the effective scattering function is random and approximates the exponential-like form only to within a fractional error $\sim N_{\text{iss}}^{-1/2}$. This scattering function will change on a time scale of about the scintillation time scale. The arrival times in Figure 5, determined from frequency-time integrations of $250 \text{ kHz} \times 32 \text{ s}$, have $N_{\text{iss}} \approx \text{few}$ so the arrival times would be expected to vary by $N_{\text{iss}}^{-1/2}\tau_d \approx 5\text{--}15 \mu\text{s}$. The arrival times vary by about $\pm 5 \mu\text{s}$ and are correlated over about 80–100 s, which is the scintillation time scale.

Figure 6 is a sequence of individual waveforms (32 s averages) in which changes in pulse shape and shifts of the pulse centroid are obvious. These show directly that the shape varies because of scintillations. We point out that *intrinsic* shape variations (due to summing a finite number of pulses), such as those that account for the phase jitter analyzed in § IIa, cannot account for the shape variations so long as the 0.43 GHz phase jitter is approximately the same as the 1.4 GHz jitter. Similarity of intrinsic phase jitter at the two frequencies seems likely, as studies of other pulsars show that intrinsic shape variations are not strongly frequency-dependent.

We also studied pulse shape variations directly by fitting various functions to the observed waveforms to obtain scattering broadening times and constrain the intrinsic widths of

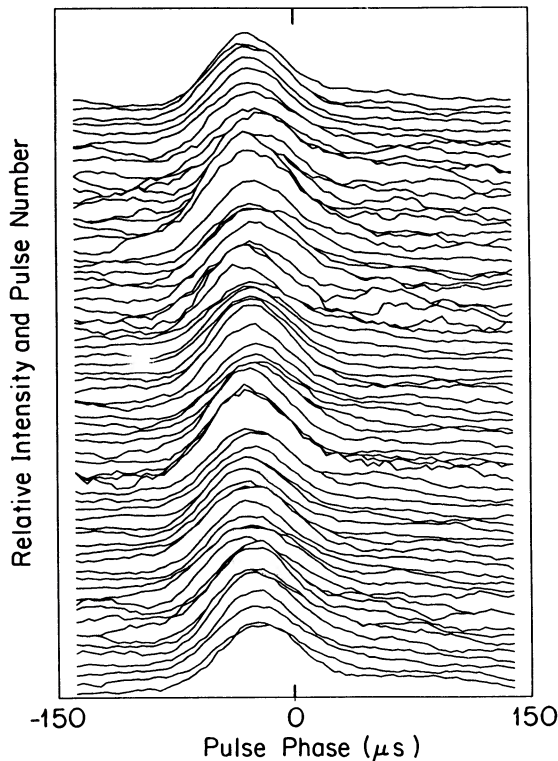


FIG. 6.—Sequence of 32 s average (2400 pulses) waveforms at 0.43 GHz, showing shape variations caused by interstellar scintillations.

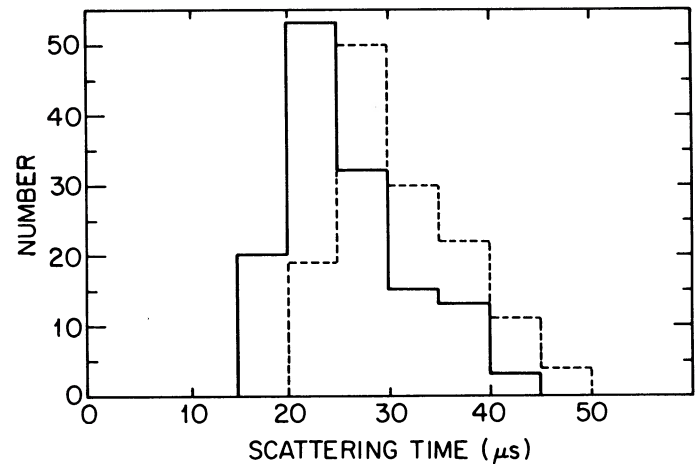


FIG. 7.—Histogram of the scattering broadening time, τ_d , for the main pulse (solid) and interpulse (dashed).

the main pulse and interpulse components. For the fits, we used a Gaussian function $\exp(-t^2/2W^2)$ convolved with a one-sided exponential $\exp(-t/\tau_d)U(t)$, U being the unit step function. The fit therefore has four free parameters, the amplitude and mean position of the Gaussian and the two width parameters, W and τ_d . We assume that the intrinsic pulse shape (the Gaussian) is time-invariant but that the scattering broadening time τ_d varies on a host of time scales.

At 430 MHz, we first made least-squares fits to determine the best value of the intrinsic width W , by minimizing χ^2 using all 1984 data. The widths are $W_{\text{mp}} = 19^{+2}_{-1} \mu\text{s}$ and $W_{\text{ip}} = 19^{+4}_{-2} \mu\text{s}$ for the main pulse and interpulse, respectively. Subsequent fits used a fixed value, $W = 19 \mu\text{s}$, for both the main pulse and interpulse. The average broadening times are $\tau_d(\text{mp}) = 25 \pm 2 \mu\text{s}$ and $\tau_d(\text{ip}) = 30 \pm 2 \mu\text{s}$ using all 1984 and 1985 data. Figure 7 shows a histogram of the decay times. The bias between main pulse and interpulse is marginally significant and may be due to a difference in the true intrinsic shapes for these two components. This is borne out from a fit (for amplitude and phase) of the interpulse to the main pulse: the interpulse at 0.43 GHz is slightly broader than the main pulse.

IV. LONG-TERM VARIATIONS

In this section we discuss scintillation and timing variations that occur on day to year time scales. The results here are predominantly empirical. In § V we interpret the results in terms of propagation effects in the interstellar medium.

a) Scintillations

Interstellar scintillations, such as those evident in the dynamic spectra of Figure 5, may be quantified through a two-dimensional correlation analysis. In Figure 8 we show two-dimensional autocorrelation functions (ACFs) of dynamic spectra obtained at two epochs. Slices along the lag axes are used to determine the scintillation bandwidth $\Delta\nu_d$ (The HWHM of the cut at zero time lag) and the scintillation time scale Δt_d (the half-width at e^{-1} of the cut at zero frequency lag). The orientation of an elliptical Gaussian function fitted to the ACF gives the drift rate dv/dt of constructive interference maxima.

The drift rate is clearly different over the interval of 7 months separating the two data sets. Drifts are due to chro-

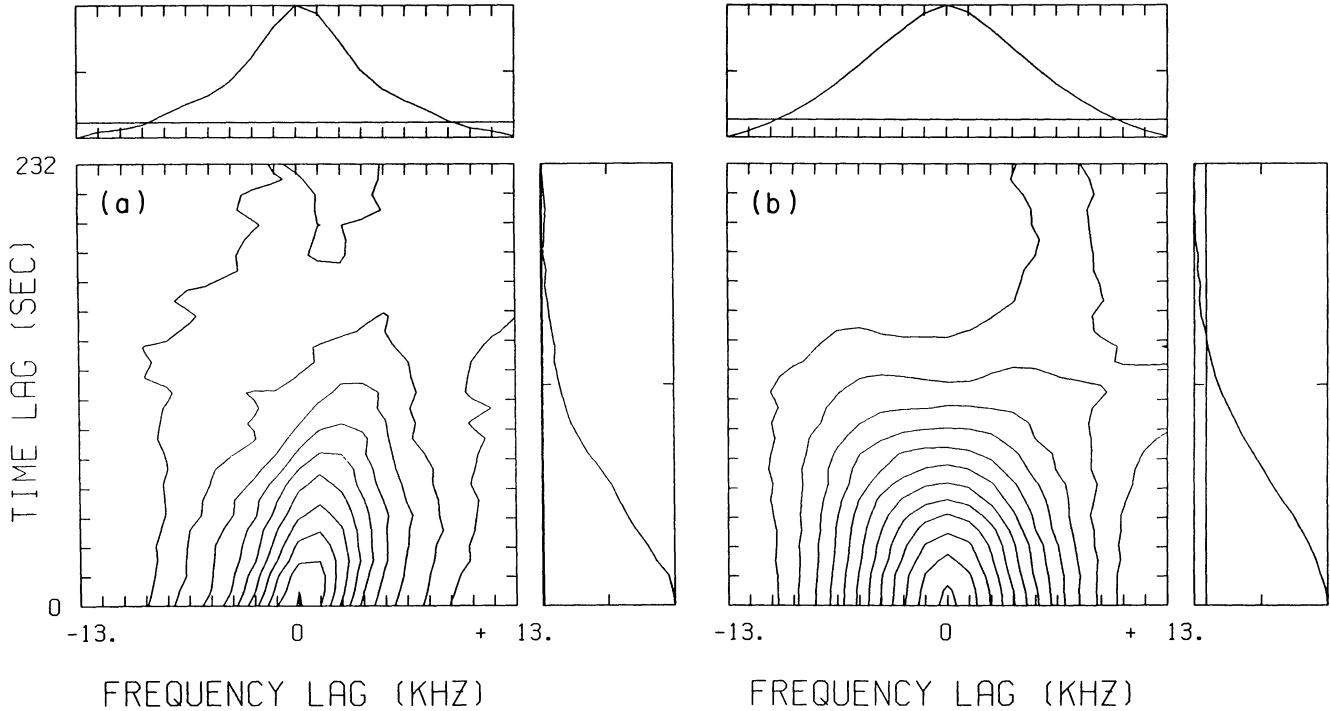


FIG. 8.—Two-dimensional autocorrelation functions of dynamic spectra with slices along the two axes. The characteristic widths in frequency ($\Delta\nu_d$) and time (Δt_d) are shown. (a) An epoch when there was significant drift of scintillation features (1984.3 = MJD 5795); (b) an epoch when there was no drift (1984.8 = MJD 6005).

matic aberration of the ray paths and signify that there are variations in electron density in the ISM on scales much larger than those that cause diffraction (Shishov 1974; Hewish 1980; CPL; Romani, Narayan, and Blandford 1986). The other scintillation parameters $\Delta\nu_d$ and Δt_d also vary with epoch. Figure 9 shows the main pulse at two epochs, where the temporal broadening time τ_d is clearly different.

The two-dimensional ACF analysis was performed on much of our 0.43 GHz data. The results are shown in Figures 10a–10c, where we plot the three scintillation parameters $\Delta\nu_d$, Δt_d and dv/dt against modified Julian date (Julian date $-24,400,000.5$). Error bars on the points are ± 1 standard deviation, where the standard deviation is estimated from several fits made at each epoch and are larger than the standard errors of the least-squares fits. For dates after MJD 6249, an effective scintillation bandwidth is plotted (*open circles*) that is derived from the temporal broadening time of the waveform using the relation $2\pi\Delta\nu_d\tau_d = 1$. All quantities vary by amounts larger than their errors on a time scale of about 200 days.

Table 2 lists scintillation parameters at 0.43 GHz averaged over all our available data. The quoted standard deviations are of the individual measurements (as opposed to of the mean), since we think that these reflect the amount by which the scintillation parameters vary from refractive effects (as discussed further in § V). Parameters at 0.32 GHz are also given from a few fits to relatively poor data. We also show results at 1.4 GHz provided by L. Rawley (private communication) and which are summarized in his Ph.D. thesis (Rawley 1986). Recall that our own data had insufficient bandwidth to allow a scintillation analysis at this frequency. Rawley provided scintillation bandwidths ($\Delta\nu_d$) and times (Δt_d) for 54 epochs from late 1984 to the end of 1986. The standard deviations in Table 2 for the 1.4 GHz data are of the *mean* scintillation bandwidth and time

(i.e., the standard deviations of individual measurements divided by the square root of the number of measurements). At 1.4 GHz, variations in the scintillation parameters appear to be due to uncorrelated estimation errors rather than to refractive scintillations, as verified by a test for whiteness on the 1.4 GHz scintillation parameters.

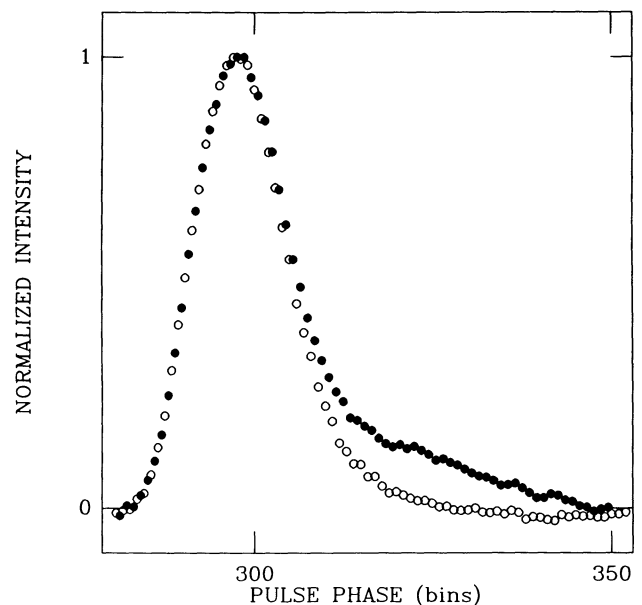


FIG. 9.—The main pulse at 0.43 GHz for two epochs showing a difference in scattering decay time: 1984.3 (*filled circles*) and 1984.9 (*open circles*).

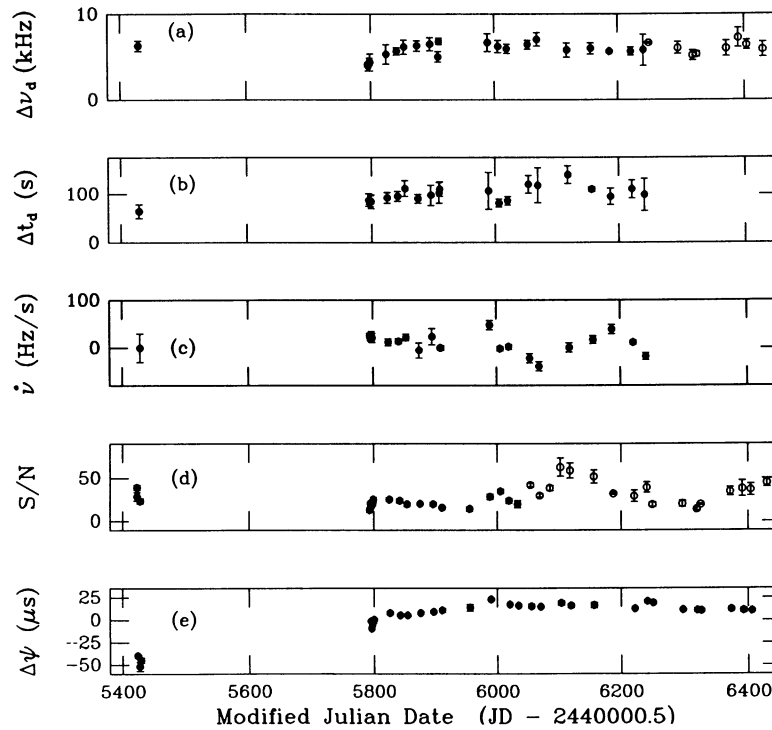


FIG. 10.—Time series of the scintillation parameters (a) $\Delta\nu_d$, where filled circles denote direct measurement of the scintillation bandwidth, open circles measurement of the pulse broadening τ_d and use of $\Delta\nu_d = 1/(2\pi\tau_d)$; (b) Δt_d , and (c) dv/dt ; (d) the signal-to-noise ratio, where open circles denote use of 125 kHz bandwidth, filled circles 250 kHz; and (e) the phase difference $\Delta\psi$ between the 1.4 GHz and 0.43 GHz arrival time data. The phase differences are with respect to the best-fit dispersion measure $DM = 71.04224$ to our 1983–1985 data. Error bars are $\pm 1\sigma$.

We also include in Table 2 the scintillation speed,

$$V_{\text{ISS}} \approx 10^{4.1} \frac{(D\Delta\nu_d)^{1/2}}{\nu\Delta t_d} \text{ km s}^{-1}, \quad (4)$$

where the constant (Cordes 1986) applies for distance D in kpc, $\Delta\nu_d$ in MHz, ν in GHz, and Δt_d in s. The scintillation speed is the magnitude of the weighted vector sum of the pulsar proper motion speed, the observatory's transverse speed, and the speed of scattering material along the line of sight. At 0.43 GHz, the scintillation speed is less than that reported by Cordes (1986), because the latter value was based on data from a single epoch with lower signal to noise ratio than the data considered here.

TABLE 2
SCINTILLATION PARAMETERS OF 1937 + 214

ν (GHz)	$\Delta\nu_d$ (kHz)	Δt_d (s)	rms dv/dt (kHz s ⁻¹)	V_{ISS} (km s ⁻¹)
0.32.....	1.4 ± 0.5	65 ± 20	...	51 ± 18
0.43.....	4.2 ± 0.9^a	100 ± 18^a	0.021	50 ± 6^b
1.40.....	923 ± 65^c	444 ± 28^c	...	42 ± 13^b

^a The errors for the 0.43 GHz data are standard deviations of the daily values in Fig. 10 which vary, in part, because of refractive variations in interstellar propagation.

^b The mean and standard deviation of the scintillation speeds are of the daily mean values.

^c Errors for the 1.4 GHz data are standard deviations of the 55 daily values supplied by L. Rawley (private communication) divided by $(55)^{1/2}$, since the variations are white noise in character and do not reflect variations caused by the interstellar medium.

The standard deviation of the velocity in Table 2 for 0.43 MHz was calculated using the 17 epochs separated by more than 15 days in order that the daily sampling in 1984 April would not bias the result unduly. The velocity standard deviation therefore reflects contributions from measurement errors, interstellar refraction (which modulates the scintillation parameters), and Earth's orbital velocity. There are insufficient data to allow a fit to the velocity curve from which one could, in principle, obtain the pulsar's vector proper motion. It is notable, however, that the fractional variation $\sigma_v/V_{\text{ISS}} = 13\%$, is less than the individual fractional variations of $\Delta\nu_d$ and Δt_d . This lends support to the view that variations in scintillation parameters are predominantly due to refraction, which modulate $\Delta\nu_d$ and Δt_d by factors that cancel in the expression for the velocity (eq. [4]). More discussion on the refractive modulation of scintillation parameters may be found in CPL.

In § V we use the scintillation data to constrain the electron density wavenumber spectrum along the line of sight to the pulsar.

b) Flux Density Variations

Figure 10d displays the waveform signal to noise ratio (SNR) at 0.43 GHz, calculated as the ratio of the waveform maximum to the rms offpulse noise. The SNRs have been corrected for the zenith angle dependence of the antenna gain and system temperature and corrected for changes in the receiver system that altered the system temperature. Thus the plotted SNR is a measure of the pulsar flux density (in arbitrary units). The plotted errors (± 1 standard deviation) are empirical errors calculated from several SNR measurements obtained at each

epoch. As with the scintillation parameters, the SNR varies with a characteristic time scale of about 200 days.

Recent work (Rickett, Coles, and Bourgois 1984; Romani, Narayan, and Blandford 1986; CPL) suggests that at least some long-term pulsar intensity variations are caused by refractive scintillations in the ISM. Moreover, there is limited evidence that *all* long term intensity variations from pulsars result from interstellar refraction. Stinebring and Condon (1990) recently observed a sample of pulsars every day for 40 days at three frequencies. Low dispersion measure (DM) pulsars showed the expected refractive variations over the 40 days while high-dispersion objects, for which the refractive time scale is well in excess of 40 days, indeed showed essentially no intensity variations.

From the time series shown in Figure 10, we obtain a modulation index for the SNR of

$$m_{\text{SNR}} \equiv \frac{\sigma_{\text{SNR}}}{\text{SNR}} = 40\% .$$

Since some of this fluctuation is undoubtedly due to estimation errors, we interpret the modulation index to be an upper bound on refractive intensity variations *over our data interval*. We predict a refraction time scale $\Delta t_r \approx (l_r/l_d)\Delta t_d \approx 1$ yr at 0.43 GHz (where $l_{r,d}$ are length scales associated with refraction and diffraction; see below) so our data span should display a good fraction of the total expected refractive fluctuation. Nonetheless, further study is warranted.

c) Arrival Time Analysis

Arrival times were obtained through conventional template fitting techniques (cf. § II) and knowledge of the time at which sampling commenced on a given day. As discussed by Davis *et al.* (1985), the observatory's rubidium standard is synchronized with the Loran C time transfer service to an accuracy of order 1 μ s. Our nominal arrival times have been corrected for variations between Loran C and the observatory clock prior to 1984 October. Beginning in 1984 October the offset between the National Bureau of Standard's estimate of UTC (transferred to the Arecibo Observatory with the Global Positioning System [GPS]) and the observatory clock has been used to correct the arrival times. Use of the GPS for pulsar timing studies is discussed by Rawley (1986) and Rawley, Taylor, and Davis (1988). Before fitting the arrival time data, they were corrected for the shift induced by scattering in the interstellar medium. As discussed in Cordes and Stinebring (1984), we estimate this shift to be 60% of the $1/e$ scattering broadening time. The net correction that was subtracted from all arrival times was then

$$\Delta t(\nu) = 0.366\nu^{-4.4} \mu\text{s} \quad (5)$$

for radio frequencies ν in GHz. In principle, this correction should be time-dependent because we have shown that the scattering broadening time varies. We have not done so in the timing results reported below because our conclusions would be largely unaffected. We will defer to another paper the results of applying a time-dependent correction.

The arrival times were fitted using the program TEMPO, courtesy of J. H. Taylor and J. M. Weisberg, and using the PEP planetary ephemeris from MIT. We fitted arrival times (referred to the solar system barycenter) using a phase model

$$\tilde{\psi}(t, \nu) = \tilde{\psi}_0 + f_0 t + \frac{1}{2} \dot{f}_0 t^2 + \frac{\delta\text{DM}}{\text{DC}} f_0 \nu^{-2} \quad (6)$$

where the tilde denotes that phase units are in cycles; f_0 and \dot{f}_0 are the spin frequency and its first derivative at the time origin; δDM is the change in dispersion measure over that assumed; and $\text{DC} = 2.41 \times 10^{-16} \text{ pc cm}^{-3} \text{ Hz}^{-1}$ is the dispersion constant for the observation frequency ν in Hz. We used a fixed value $\text{DM} = 71.0440 \text{ pc cm}^{-3}$ (Cordes and Stinebring 1984) to reference the arrival times to infinite frequency. In translating to the solar system barycenter, the right ascension and declination were assumed equal to those published by Rawley (1986), and the proper motion was assumed to be zero.

The fit to all 0.43 and 1.4 GHz data from 1983 through 1985 yields a best-fit dispersion measure $\text{DM} = 71.04224 \pm 0.00005 \text{ pc cm}^{-3}$ (± 1 standard error). In Figure 10 we show the phase differences (in temporal units)

$$\Delta\psi(t, 0.43 \text{ GHz}, 1.4 \text{ GHz}) \equiv f_0^{-1} [\tilde{\psi}(t, 1.4 \text{ GHz}) - \tilde{\psi}(t, 0.43 \text{ GHz})] \quad (7)$$

between the 0.43 and 1.4 GHz data, expressed in time units; note that these differences are with respect to the best-fit DM.

Like all other quantities plotted in this figure, the phase difference varies smoothly with time. Errors in the mean phase difference at each epoch were calculated from the observed variations of individual pairs of 0.43 and 1.4 GHz fits and errors are dominated by scintillation induced variations in the 0.43 GHz data (cf. § IIa).

d) Frequency-dependent TOA Perturbations

Are the frequency-dependent TOA variations caused solely by changes in dispersion measure? In Figure 11 we show $\Delta\psi(t, \nu, 1.4 \text{ GHz})$ plotted against $\nu^{-2} - (1.4 \text{ GHz})^{-2}$ for the two epochs, MJD 5426 (1983.3) and MJD 6027 (1984.9). At the earlier epoch, data at frequencies 0.32, 0.43, and 1.4 GHz are plotted while the second epoch has data at 0.43, 0.61, and 1.4 GHz. The errors on the data points are $\pm 1 \sigma$. Also shown are least-squares fits of straight lines that pass through the origin, whose slopes are proportional to the dispersion measure perturbations. For the first epoch, the data points are completely consistent with the fit, which gives $\chi^2/\sigma^2 \approx 0.5$ compared to an expected value of unity for a fit using 2 pairs of frequencies. In our earlier paper (Cordes and Stinebring 1984), we demonstrated that the frequency-dependent timing variations were consistent with those caused by dispersion for this epoch. At the second epoch some 1.6 yr later, the data and fit appear to be inconsistent, giving $\chi^2 \approx 5$, suggesting the presence of additional frequency-dependent TOA perturbations. It is possible that some or all of this perturbation is really due to the refraction-induced modulation of the scattering broadening time (τ_d). In our analysis, we corrected arrival times using a best *mean* value of τ_d , as discussed above, but we did not correct for the $\sim 20\%$ variations in τ_d . These variations would introduce $\sim 3 \mu\text{s}$ perturbations in the 0.43 GHz arrival times which, if corrected, might reduce χ^2 to about unity.

To explore further the frequency dependence of TOA perturbations, we compare our data with those of Rawley (1986) and Rawley, Taylor, and Davis (1988). Expressing our 1.4-0.43 GHz phase differences as dispersion measure perturbations, we obtain the values shown as filled circles in Figure 12. We also show a measurement obtained in 1988 November (MJD = 7477) obtained by one of us (J. M. C.) and R. Foster. Rawley *et al.* made observations at 2.4 and 1.4 GHz and detected frequency-dependent phase variations that they expressed as dispersion measure perturbations $\delta\text{DM} \approx 0.001$

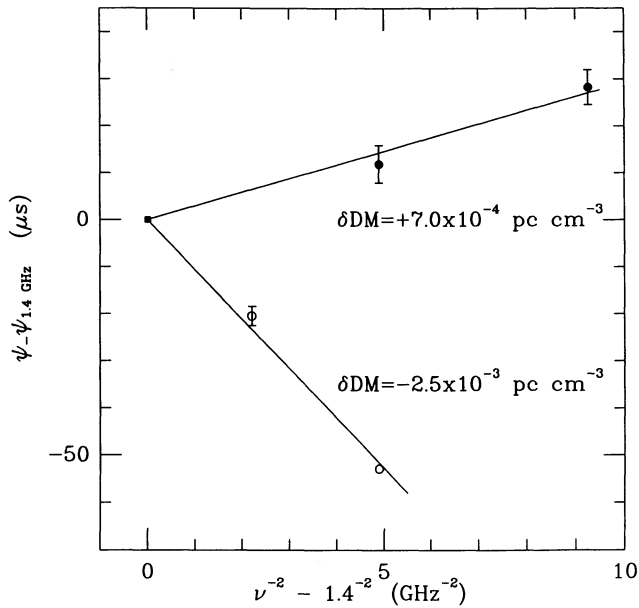


FIG. 11.—Residual pulse phase differences plotted against difference in ν^{-2} for pairs of frequencies. Data from two epochs are shown: 1983.3 = MJD 5423 (filled circles) and 1984.9 = MJD 6027 (open circles). The solid lines are least-squares fits to lines that pass through the origin and whose slopes are proportional to δDM , the dispersion measure perturbation, as shown. The perturbations in dispersion measure are with respect to $\text{DM} = 71.0440$. Error bars ($\pm 1\sigma$) are shown only where they are larger than the plotted point.

pc cm^{-3} . We show these in Figure 12 as open circles. It is obvious from Figure 12 that, for epochs in common between the two data sets (i.e., 1985), the dispersion measure variations differ both in their variations and in their mean values. The

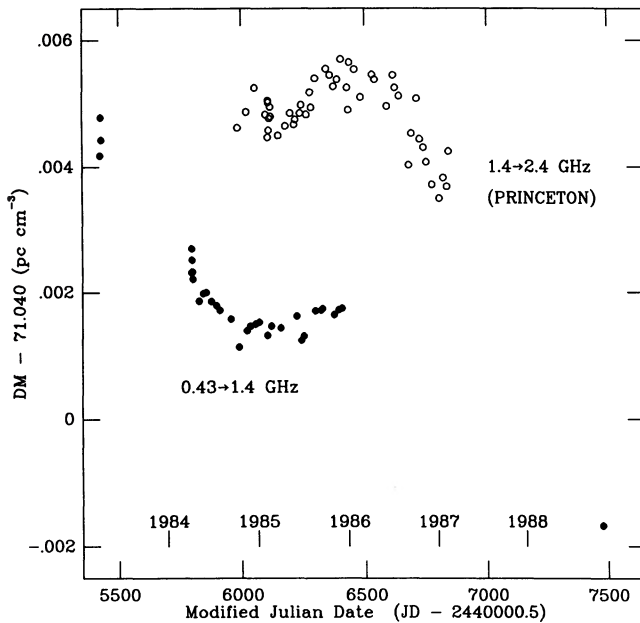


FIG. 12.—Estimates of dispersion measure plotted against time. These estimates are derived solely from pairs of frequencies and may reflect other contributions to arrival time differences. Filled circles derive from 0.43 and 1.4 GHz phase differences (this paper) and open circles derive from 1.4 and 2.4 GHz phase differences (Rawley, Taylor, and Davis 1988).

bias in mean DM is about $0.0035 \text{ pc cm}^{-3}$ between the two sets of measurements. This could be accounted for if the 0.43–1.4 GHz phase differences are systematically in error by about $70 \mu\text{s}$, or if the 1.4–2.4 GHz phase differences are in error by about $5 \mu\text{s}$, or if all phase differences are in error. The time variations in DM for 1985 are slightly smaller in the low-frequency data (0.43–1.4 GHz), but when the 1983 and 1984 data are included, the variations are much larger than implied by the extended 1.4–2.4 GHz data set shown in Rawley *et al.* (1988). If the bias between the two sets of data is removed, the 1985 variations in DM are similar, and recent data taken at 1.4 and 2.4 GHz (J. H. Taylor, private communication) are consistent with the 1988 November data point in Figure 12. Thus, at least qualitatively, the overall variation in DM appears similar between the two data sets. It remains to be seen whether *all* variations are the same. A definitive and quantitative analysis will be deferred to another paper.

At the present time, the source of bias and difference in DM variation cannot be determined with certainty. Some plausible explanations for the bias and variation in DM can be advanced, however. Bias in dispersion measure estimates made at low and high frequencies might be due to the following:

1. A change in pulse shape with frequency, such as the decrease with frequency of the separation of main and interpulse that we have found or changes in amplitude ratio of subcomponents of the main pulse, for example. These amplitude changes are seen in almost all pulsars (e.g., Hankins and Rickett 1986) and are probably related to the efficacy of the coherent radiation process. Bias due to shape changes is a much larger error in the 1.4–2.4 GHz data, since the required bias is about $5 \mu\text{s}$, a small fraction of the $45 \mu\text{s}$ pulse width. The required bias at low frequency ($70 \mu\text{s}$) is too large to be accounted for by a change in pulse shape.

2. Frequency-dependent propagation effects other than simple changes in dispersion measure. Such effects may be related to angle of arrival fluctuations associated with refraction in the ISM. We discuss this possibility in § V.

3. Dispersion measure changes that result when observations at different frequencies sample different irregularities in the ISM. Different sampling would result from the difference in size of the 0.43 and 1.4 GHz interstellar scattering disks, which are $\approx 3 \text{ mas}$ and $\approx 0.3 \text{ mas}$, respectively, corresponding to a factor of 100 difference in solid angle.

4. A breakdown in the assumption that all radio frequencies are emitted from the same altitude or from the same rotational phase of the pulsar. A variation of emission frequency with altitude is expected to produce arrival time shifts from some combination of aberration and retardation effects (Cordes 1978; Matese and Whitmire 1980) and magnetic field line distortion (e.g., Shitov 1984). Beaming of radiation toward the observer may also be frequency-dependent through refraction in the magnetosphere (Melrose 1979; Barnard and Arons 1986) or through a combination of a radius to frequency mapping, gravitational bending of rays (Cordes 1981), and reference frame drag (Kapoor and Datta 1986).

Similar explanations may account for the variations in dispersion measure once the bias is accounted for. Another possibility for a difference in variation is if the pulsar spin axis undergoes free or forced precession and the pulsar radiation beam is frequency dependent.

In § V we discuss the timing results in greater detail and use them to constrain electron density variations in the interstellar medium.

V. CONSTRAINTS ON THE INTERSTELLAR ELECTRON DENSITY POWER SPECTRUM

Let $P_{n_e}(\mathbf{q})$ be the electron density power spectrum as a function of wavenumber \mathbf{q} , normalized such that the integral over three-dimensional wavenumber volume ($d^3\mathbf{q}$) is the mean square electron density. It is conventional to express the spectrum as a power law over a finite wavenumber range that depends on the magnitude of \mathbf{q} (isotropic statistics):

$$P_{n_e}(\mathbf{q}) = C_n^2 q^{-\alpha}, \quad q_0 \leq q \leq q_1. \quad (8)$$

The wavenumber cutoffs for the irregularities define an "inner" scale $l_1 \equiv 2\pi/q_1$ and an "outer" scale $l_0 \equiv 2\pi/q_0$. There is evidence that the outer scale is many orders of magnitude larger than the inner scale (Lee and Jokipii 1976; Armstrong, Cordes, and Rickett 1981).

Scintillation and scattering data from pulsars and other sources have been used for (1) determining C_n^2 to study the Galactic distribution in the level of "turbulence" (Cordes, Weisberg, and Boriakoff 1985, hereafter CWB; Alurkar, Slee, and Bobra 1986; Spangler, Fey, and Cordes 1987); (2) estimating the index α from the scaling with frequency of the scintillation parameters and from the shapes of visibility functions under various assumptions about the wavenumber cutoffs (CWB; Goodman and Narayan 1985, 1989; Wilkinson, Spencer, and Nelson 1988; Gwinn, Moran, and Reid 1988; Spangler and Cordes 1988); and (3) estimating the upper wavenumber cutoff, q_1 , assuming that it is comparable to inverse length scales relevant to the optics, such as the reciprocal of the Fresnel scale (Coles *et al.* 1987).

a) Distribution of Scattering Material along the Line of Sight

The level of scattering C_n^2 (averaged over the line of sight) may be estimated as (cf. eq. [6] of CWB)

$$\overline{C_n^2} = 6A_x \nu^\alpha D^{-\alpha/2} \Delta\nu_d^{-(\alpha-2)/2} \approx 0.002\nu^{11/3} \times D^{-11/6} \Delta\nu_d^{-5/6} (\text{m})^{-20/3}, \quad (9)$$

where A_x is a constant given by equation (A10) of CWB and the expression after the approximate equality is applicable to the case where $\alpha = 11/3$ (the "Kolmogorov" value); ν is in units of GHz; $\Delta\nu_d$ in MHz; and distance D in kpc. The level of scattering toward PSR 1937+214 is modest, despite its attributed distance (Heiles *et al.* 1983) of 5 kpc: $C_n^2 \approx 10^{-3.5} \text{ m}^{-20/3}$, a value that is among the smallest seen from pulsars. Values of C_n^2 range up to 10^4 times larger than that seen from 1937+214, with the largest values associated with clumps of strong turbulence (Dennison *et al.* 1984; CWB). It seems probable, then, that the scattering material is nearly homogeneously distributed along the line of sight to 1937+214. This is consistent with a comparison between the measured angular diameter (C. R. Gwinn *et al.* 1990, in preparation) and the angular diameter predicted from the pulse broadening τ_d and assuming a homogeneous distribution.

b) Relevant Length Scales

In the following we refer to several length scales that can be inferred from the pulse broadening time τ_d of PSR 1937+214. Assuming that scattering material fills the line of sight uniformly, the scattering diameter is

$$\theta_{\text{FWHM}} = \left(\frac{16 \ln 2 c \tau_d}{D} \right)^{1/2}. \quad (10)$$

Equation (10) is general in relating the net differential time delay to the observed angular broadening; it does not depend

on any particular form for the wavenumber spectrum of the medium. The diffraction scale is the characteristic size of intensity maxima that are swept across the line of sight to produce fast intensity variations:

$$l_d \approx (2 \ln 2)^{1/2} \left(\frac{\lambda}{\pi \theta_{\text{FWHM}}} \right), \quad (11)$$

and is $2^{1/2}$ smaller than the $1/e$ half-width of the visibility function.

Refractive intensity scintillations are associated with scales that are much larger than those responsible for the diffraction. For a wavenumber spectrum of the form of equation (8) with $\alpha \approx 11/3$, the refraction scale is the size of the scattering disk at a point midway between Earth and the pulsar (Rickett, Coles, and Bourgois 1984):

$$l_r = D \theta_{\text{FWHM}} / 2. \quad (12)$$

For 1937+214 at 0.43 GHz, equations (10)–(12) yield

$$\begin{aligned} \theta_{\text{FWHM}} &\approx 4.7 \text{ mas}, \\ l_d &\approx 10^{9.1} \text{ cm}, \\ l_r &\approx 10^{14.3} \text{ cm}. \end{aligned}$$

The inner and outer scales of the scattering medium may have nothing to do with the "observed" length scales, l_d , l_r . However, observations of various effects can be used to infer *bounds* on the inner and outer scales, as we show below.

c) Determinations of the Spectral Index α

Recent work on interstellar scintillations has distinguished *diffractive* from *refractive* scintillations, which are responsible for short-term (~ 100 s) and long-term (~ 100 day) intensity variations of pulsars, respectively. Our understanding of scintillation theory is such that, given the power spectrum of the electron number density (n_e), the *ensemble average* moments of intensity variations, time of arrival fluctuations, and scintillation parameters can readily be calculated. The inverse problem of constraining the power spectrum of n_e from a *finite* amount of data involves a number of uncertainties, however, (CPL; Narayan 1988).

One uncertainty is that inversion formulae are sometimes double-valued. An example is the scaling of scintillation bandwidth $\Delta\nu_d$ with observation frequency. If expressed as

$$\Delta\nu_d \propto \nu^{x_\nu}, \quad (13)$$

the spectral index α may be solved for using equations (50) and (56) of CPL (which hold for $l_1 \ll l_d \ll l_r \ll l_0$)

$$x_\nu = \begin{cases} \frac{2\alpha}{\alpha-2} & 2 < \alpha < 4 \\ \frac{8}{6-\alpha} & 4 < \alpha < 6. \end{cases} \quad (14)$$

The minimum value of x_ν is 4 for $\alpha = 4$ and values of α both greater than and less than 4 can account for $x_\nu > 4$.

A similar scaling holds for the scintillation times scale. Letting $\Delta t_d \propto \nu^{x_t}$ we find from equations (48) and (55) of CPL (with the same restrictions on the inner and outer scales) that

$$x_t = \begin{cases} \frac{2}{\alpha-2} & 2 < \alpha < 4 \\ \frac{\alpha-2}{6-\alpha} & 4 < \alpha < 6. \end{cases} \quad (15)$$

Despite these twofold ambiguities, however, it seems possible to distinguish “steep” ($\alpha > 4$) from “shallow” ($\alpha < 4$) power laws, because the former are expected to produce much stronger refractive effects than the latter. This is true so long as $l_0 \gg l_r$. Refraction effects include strong flux variations, modulations of the scintillation parameters, and time of arrival variations.

d) Scaling of Scintillation Parameters with Frequency

The scaling of scintillation bandwidth and time scale with frequency provide independent estimates of the spectral index α of $P_{nc}(q)$. We use the 0.43 and 1.4 GHz data in Table 2, since they have been averaged over about 2 yr and the quality is much higher than the 0.32 GHz data. The bandwidth scaling is $x_v = 4.58 \pm 0.2$ which implies spectral indices (labeled with “v” to denote use of scintillation bandwidth) $\alpha_v = 3.55 \pm 0.11$ or $\alpha_v = 4.25 \pm 0.08$ using the shallow and steep power-law expressions, respectively, in equation (14). Similarly, the 0.43 and 1.4 GHz values for scintillation time scale in Table 2 yield from equation (15) $x_t = 1.27 \pm 0.16$, which implies spectral indices (now labeled with “t”): $\alpha_t = 3.58 \pm 0.2$ or $\alpha_t = 4.24 \pm 0.12$.

The values of α obtained using the independent scintillation quantities agree with each other, to well within the errors. The 0.32 GHz data are completely consistent with these results.

e) Modulation Indices of Scintillation Parameters

It appears that additional quantities may be used to resolve the twofold ambiguity in determining the spectral index α from frequency scaling laws. Pidwerbetsky (1988) evaluated the modulation indices (i.e., the standard deviation divided by the mean) of scintillation parameters from simulations of wave propagation through media with power spectra of the form of equation (8). He considered single-phase screens, as in CPL, and sequences of 16 screens along the line of sight. He also considered power spectra where the upper wavenumber cutoff was comparable to the Fresnel wavenumber, $q_F \equiv 2\pi/(\lambda D)^{1/2}$, a case that Coles *et al.* (1987) argue to be relevant to the interstellar medium. Pidwerbetsky’s simulations indicate that the modulation indices of (1) scintillation bandwidth Δv_d ; (2) scintillation time scale Δt_d ; (3) scintillation velocity V_{ISS} ; and (4) flux density are all sensitive to the spectral index, the wavenumber cutoff, q_1 , and the thickness of the medium. In the strong scattering regime (in particular, at a frequency that is one-sixth of the frequency where the diffractive intensity modulation index is 50%, as in CPL), a single-phase screen with $q_1 \gg q_F$ produces the minimum modulation indices for all four quantities for fixed α . For $\alpha = 11/3$, the Kolmogorov case, all modulation indices are about 10%–20% while for $\alpha = 4.25$ they are about 40%–50%. Multiple-phase screens along the line of sight increase the modulation indices over those for a single-phase screen (with the same net scintillation bandwidth) for all values of α . A decrease in q_1 toward the Fresnel wavenumber q_F also increases the modulation indices.

It is therefore significant that the fractional standard deviations of the scintillation time and frequency scales and velocity in Table 2 are all less than 20%. These are upper bounds on refractive fluctuations in our observed time span, because estimation errors are included. It might be argued that the variations are underestimated in the 0.43 GHz data owing to the finite time span. However, the expected refractive time scale $\Delta t_r \approx 1$ yr suggests that the refraction is adequately sampled by our data. It would clearly be better to have a longer time

span of data, but we would consider it fortuitous if the 1984 and 1985 data were not representative. There are several kinds of media that can give large values of modulation index, but only the shallow power laws give small values. Therefore, we conclude that the wavenumber spectrum is shallow, $\alpha < 4$, for the line of sight to PSR 1937+214 and the empirical scalings of Δv_d and Δt_d with frequency imply $\alpha = 3.55 \pm 0.11$, for which the Kolmogorov value of 11/3 is completely consistent.

f) Drift Rates and Refraction Angles

Drifts of constructive maxima in dynamic spectra are caused by electron density irregularities that are larger than the refraction scale l_r . The drift rate may be expressed, for a single screen, as (CPL, eq. [28], with a slight correction):

$$\frac{dv}{dt} = \frac{vV_{\perp}}{2D\hat{v} \cdot \theta_r}, \quad (16)$$

where θ_r is the (two-dimensional) refraction angle produced by large-scale irregularities and \hat{v} is a unit vector pointing in the direction of the pulsar proper motion.

Variations in drift rate, normalized by the diffractive scintillation parameters, may be used to constrain the extent to which the pulsar image wanders as a result of time variable refraction. CPL (eq. [60]) define the quantity

$$r = \frac{\sigma_{\theta_r} \sqrt{2}}{\theta_{FWHM}}, \quad (17)$$

which is the ratio of the rms refraction angle in a single dimension to the scattering diameter, θ_{FWHM} . For shallow wavenumber spectra, this ratio is small (10%–20%), while for steep spectra, it can exceed unity. The ratio may also be related to variations in drift rate. Using equation (68) of CPL and assuming that the standard deviation of dv/dt is approximately equal to the reciprocal of the standard deviation of dt/dv , we obtain

$$r \approx \frac{\Delta v_d}{4(\ln 2)^{1/2} \sigma_{dv/dt} \Delta t_d}. \quad (18)$$

At 0.43 GHz, for which the scintillations of 1937+214 are best analyzed, we estimate $r \approx 15\%$ from Table 2, indicating that refractive wandering of the image is expected to be much less than diffractive smearing of the pulsar image. For a Kolmogorov spectrum, equation (61) of CPL yields a *predicted* ratio

$$r = 0.75 \left(\frac{\Delta v_d}{v} \right)^{1/6} \approx 11\%,$$

which is entirely consistent with the observed changes in drift rate. It might be argued that the standard deviation of dv/dt is underestimated in our 0.43 GHz data owing to the finite time span. However, the expected refractive time scale $\Delta t_r \approx 1$ yr suggests that the refraction is adequately sampled by our data.

g) Dispersion Measure and Angle of Arrival Variations

The interstellar medium perturbs pulse arrival times owing to changes in dispersion measure and to angle of arrival variations of the pulsar signal. There are three terms in the net perturbation which have distinct variations in time and frequency.

Dispersion measure variations are directly related to the phase perturbation imposed on electromagnetic waves by elec-

tron density variations along the line of sight. Letting this perturbation (in radians) be $\phi(x)$ (in a one-dimensional model with the relative Earth-pulsar velocity oriented along the x -axis), the TOA perturbation (in time units) is

$$\psi_{\text{DM}} = (2\pi\nu)^{-1}\phi(x) \quad (19)$$

and has the usual ν^{-2} scaling with frequency (Lovell 1970; Armstrong 1984; Blandford, Narayan, and Romani 1984; CPL; Rickett 1988).

Angle of arrival variations impose two kinds of TOA perturbation. The first is due to the change in geometrical path length. For a thin screen that refracts ray paths through an angle $\theta_r(x) = (\lambda/2\pi)(d\phi/dx)$, this TOA perturbation is

$$\psi_g \approx D\theta_r^2(x)/2c \quad (20)$$

for a pulsar at distance D and scales as ν^{-4} . The second kind arises when topocentric arrival times are referred to the solar system barycenter using an assumed direction to the pulsar (Backer 1986). Angle of arrival variations cause the true direction to differ from the assumed direction, thus introducing a perturbation similar to that caused by proper motion of the pulsar (e.g., Manchester, Taylor, and Van 1974) but which scales with frequency as ν^{-2} . The “iss proper motion” term has the form

$$\psi_{\text{isspm}} = \frac{(1 \text{ AU})}{c} [\hat{n}(t) - \hat{n}_{\text{assumed}}] \cdot \hat{r}_e \quad (21)$$

where $\hat{n}(t)$ is a unit vector pointing from the barycenter to the apparent direction to the pulsar while \hat{n}_{assumed} is the assumed direction. The unit vector \hat{r}_e points from the barycenter to the observatory. It is clear that ψ_{isspm} oscillates with a yearly period and is amplitude modulated by a randomly varying refraction angle $\theta_r(t)$.

The net perturbation of arrival times by interstellar effects is the sum of three terms that have different time dependences: the frequency dependences are such that two vary as ν^{-2} and one as ν^{-4} for discrete clouds of ionized plasma. As stated before, the scaling laws for a *spectrum* of irregularities are more complex. CPL and Romani, Narayan, and Blandford (1986) have estimated the amplitudes of the dispersive and geometric terms (eqs. [19] and [20]). Using Table 1 of CPL, an assumed distance (Heiles *et al.* 1983) of 5 kpc, and the derived value of C_n^2 , we can estimate the difference in arrival time perturbations at two epochs separated by time τ . For easy reference to other work, we will use the scaling laws for a Kolmogorov spectrum ($\alpha = 11/3$). The rms deviation of the dispersive variations is

$$\sigma_{\psi_{\text{DM}}}(\tau) = 2.9 \mu\text{s} (v_{50} \tau_{\text{yr}})^{5/6} v_{\text{GHz}}^{-2}$$

and grows with increasing τ up to a maximum time $\tau_{\text{max}} = l_0/V$ which could be as long 10^4 yr for an outer scale of 1 pc. Geometric path length differences have a *maximum* rms deviation

$$\sigma_{\psi_g} = 0.44 \mu\text{s} v_{\text{GHz}}^{-49/15}$$

¹ Strictly speaking, the frequency dependence is ν^{-4} only if refraction is caused by a “blob” of size much larger than the refraction scale l_r . For media containing a power-law spectrum of irregularities, the frequency dependence is different. See, for example, the scaling laws for refraction angle in Tables 1 and 2 in CPL and Table 1 of Romani, Narayan, and Blandford 1986. The same is true for the frequency dependence of any angle of arrival effect. We will use the dependences for a discrete “blob” since they characterize the basic physical effects.

that is reached for lags longer than the refraction time scale $l_r/V \approx 0.2 \text{ yr } v_{\text{GHz}}^{-1/15}$ and varies linearly in τ for shorter lags.

Using these scaling laws, one can show that both the dispersive and geometric perturbations are important at 0.43 GHz while only the former is the dominant effect at 1.4 GHz and higher frequencies. At 0.43 GHz the dispersive variations are predicted to be about 39 μs for the 1000 day span of our 1983–1985 data, compared to an actual variation (Fig. 10) of 75 μs . The difference may not be significant given that there are very few independent samples of the dispersive variations in our data set. Also, we have previously shown that the frequency-dependent variations in time of arrival are consistent with changes in dispersion measure.

h) The Interstellar Phase Structure Function

In his dual frequency timing study of PSR 1937+214, Rawley (1986) detected frequency-dependent variations in arrival time that he *expressed* as changes in dispersion measure. Rickett (1988) analyzed Rawley’s data under the assumption that they reflected DM variations (plus measurement errors) and used them to constrain the interstellar phase structure function. Here, we apply Rickett’s analysis to our own data and compare the result with Rawley’s data. In § IVc we demonstrated that there is significant bias between values of DM calculated from Rawley’s data (1.4 and 2.4 GHz) and our data (0.43 and 1.4 GHz). We tacitly assume that this bias is probably due to a slight frequency difference between the 1.4 and 2.4 GHz pulse shapes. In spite of this bias, it is arguable that fluctuations about the mean DMs may be used to probe the properties of the interstellar medium.

The phase structure function (again, for a thin screen medium) as a function of spatial lag b is

$$D_\phi(b) = \langle [\phi(x+b) - \phi(x)]^2 \rangle \quad (22)$$

for the one-dimensional phase model and where angular brackets denote an ensemble average. In the following, we relate spatial lags b to time lags τ by $b = V\tau$, under the common assumption that density variations in the medium are “frozen in” and are simply convected across the line of sight. Therefore, we will henceforth use τ as the argument to all structure functions.

Assuming that TOA variations at a given frequency are *solely* due to dispersion measure variations, it is simple to relate the phase structure function to the structure function of the TOA variations. Our observable, however, is the *difference* in phase (expressed in time units) between two frequencies ν_1 and ν_2 at an epoch t :

$$\Delta\psi(t, \nu_1, \nu_2) = \psi(t, \nu_2) - \psi(t, \nu_1) \quad (23)$$

The structure function of $\Delta\psi$ is

$$D_{\Delta\psi}(\tau, \nu_1, \nu_2) \equiv \langle [\Delta\psi(t, \nu_1, \nu_2) - \Delta\psi(t + \tau, \nu_1, \nu_2)]^2 \rangle, \quad (24)$$

and it may be related to the phase structure function at an arbitrary frequency ν by

$$D_\phi(\tau, \nu) = \left[\frac{2\pi(\nu_1 \nu_2)^2}{\nu(\nu_2^2 - \nu_1^2)} \right]^2 [D_{\Delta\psi}(\tau, \nu_1, \nu_2) - 2\sigma^2(1 - \delta_{\tau,0})] \quad (25)$$

where σ is the standard deviation of additive measurement errors in $\Delta\psi(t, \nu_1, \nu_2)$ and the Kronecker delta $\delta_{\tau,0}$ ensures that the bias $2\sigma^2$ is subtracted only for nonzero lags. Additive measurement errors are assumed to be statistically independent between observations because they are dominated by pulse

jitter and radiometer noise (cf. § IIIb). Subtraction of the bias is an important source of error in our estimates of the phase structure function.

To estimate the TOA structure function D_ψ , we have used the sum

$$\hat{D}_\psi(\tau, \nu_1, \nu_2) = \frac{1}{N(\tau)} \sum_{j,k} [\Delta\psi(t_j, \nu_1, \nu_2) - \Delta\psi(t_k, \nu_1, \nu_2)]^2, \quad (26)$$

where values of j, k are restricted to $\tau - \Delta\tau \leq |t_j - t_k| \leq \tau + \Delta\tau$. Similar estimators have been used by Rickett, Coles, and Bourgois (1984), Simonetti, Cordes, and Heeschen (1985), and Cordes and Downs (1985). The bin sizes $\Delta\tau$ in lag τ have been chosen so that the number of terms $N(\tau)$ in the sum for each lag is at least 10. This requires, given the irregular sampling, that the bin sizes vary with lag. The structure function is the mean of the summand in equation (26). Errors in the structure function estimates have been calculated by finding the standard deviation of the summand and dividing by $N_{\text{data}}(\tau)^{1/2}$, where $N_{\text{data}}(\tau)$ is the number of *data* points contributing to the sum, not the number of terms in the sum (cf. Simonetti, Cordes, and Heeschen 1985). We therefore assume that data points are statistically independent, which is true only under the null hypothesis that the data contain only noise and no correlated TOA variations.

In Figure 13 we show the phase structure function that results from the assumption that all TOA variations are due to DM variations and measurement error. The structure function is evaluated at a frequency $\nu = 1.4$ GHz, which is the frequency that is common to both Rawley's data and our own and was

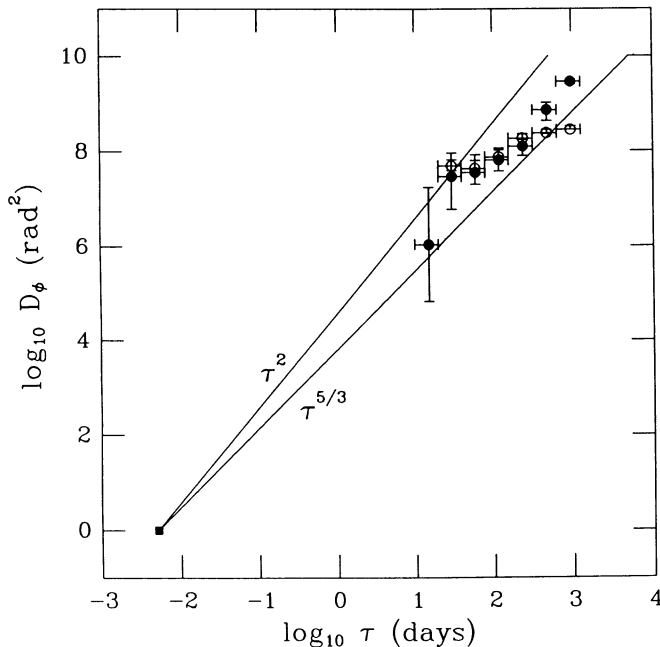


FIG. 13.—Estimates of the interstellar phase structure function at 1.4 GHz based on time of arrival variations and on the diffractive scintillation time scale. Filled circles depict estimates based on the 0.43 and 1.4 GHz arrival time variations in Fig. 10 (using data only before MJD 7000), while open circles are based on the 1.4 and 2.3 GHz data of Rawley (1986). The filled square is the diffractive scintillation time scale, corresponding to the scale on which the phase structure function is unity. Following Rickett (1988), the solid lines represent theoretical scalings of τ^2 and $\tau^{5/3}$ that are expected for wavenumber spectra (cf. eq. [8]) with exponents α equal to 4 and 11/3, respectively.

also used by Rickett in his analysis of Rawley's data. Filled circles represent estimates based on our 0.43 and 1.4 GHz data while open circles depict estimates based on Figure 4-2 of Rawley (1986). Error bars are $\pm 1 \sigma$. In addition to constraining the structure function for lags of tens to hundreds of days, diffractive scintillations may be used to evaluate D_ϕ for a time scale equal to the scintillation time scale. The intensity autocovariance due to diffractive scintillations may be expressed as (Rickett 1977)

$$\Gamma_I(\tau) \equiv \langle I(t)I(t + \tau) \rangle = \exp[-D_\phi(\tau)], \quad (27)$$

a result that holds in the strong scintillation regime, which is defined as (scintillation bandwidth) \ll (observation frequency) and is applicable to all data for PSR 1937+214. According to equation (27) the $1/e$ scintillation time scale is by definition the scale on which the phase structure function is unity. Therefore, we have plotted the 1.4 GHz scintillation time scale (cf. Table 2) in Figure 13 as a square symbol.

The interpretation of Figure 13 is difficult. Most points fall between the two theoretical curves $D_\phi(\tau) \propto \tau^2$ and $\tau^{5/3}$, scaling laws that apply for electron density wavenumber spectra (cf. eq. [8]) with $\alpha = 4$ and $\alpha = 11/3$, respectively, and under the condition that $V\tau q_0 \ll 1 \ll V\tau q_1$ (where V is the relative, transverse Earth-pulsar speed). For lags in common to Rawley's and our own data set, estimates of the structure function agree. The agreement would suggest that arrival time variations do, in fact, scale as ν^{-2} as has been assumed in equation (19). However, our own data provide estimates for larger lags which suggest that the variations at lower frequencies diverge from those measured at high frequencies. This may imply the presence of TOA variations that vary more strongly with frequency than the ν^2 dependence.

Another difficulty in interpreting the structure functions *solely* in terms of DM variations is the fact that at the small lags (e.g., 10–100 days), the structure function scales with τ much more slowly than even $\tau^{5/3}$, suggesting either that the bias in the structure functions has been underestimated or that additional contributions to TOA variations are present. These additional TOA variations may arise from other propagation-induced variations, such as the angle of arrival effects discussed above, or from effects intrinsic to the pulsar that depend on frequency.

In conclusion, the frequency dependence of the TOA variations is at best poorly constrained. At the least, however, we may conclude that long-term TOA variations are present in the data and they are *roughly* consistent with those expected from the same sort of electron density wavenumber spectrum that accounts for diffractive scintillations on time scales that are four to five orders of magnitude shorter. There seems to be no evidence in our data or Rawley's data for the large TOA variations that are expected for steep power laws with $\alpha > 4$ (e.g., Goodman and Narayan 1985).

i) The Electron Density Wavenumber Spectrum

The results of this section are summarized in Figure 14, where we show bounds on the wavenumber spectrum that derive from our determination of the spectral index $\alpha = 3.55 \pm 0.11$, the scintillation bandwidth $\Delta\nu_d$, the diffraction and refraction scales l_d and l_r , and use of equation (9). This spectrum is similar to that proposed by Armstrong, Cordes, and Rickett (1981), who synthesized data on many pulsars to show that the high-wavenumber portion of the spectrum (sampled by scintillation phenomena) extrapolates well to low-

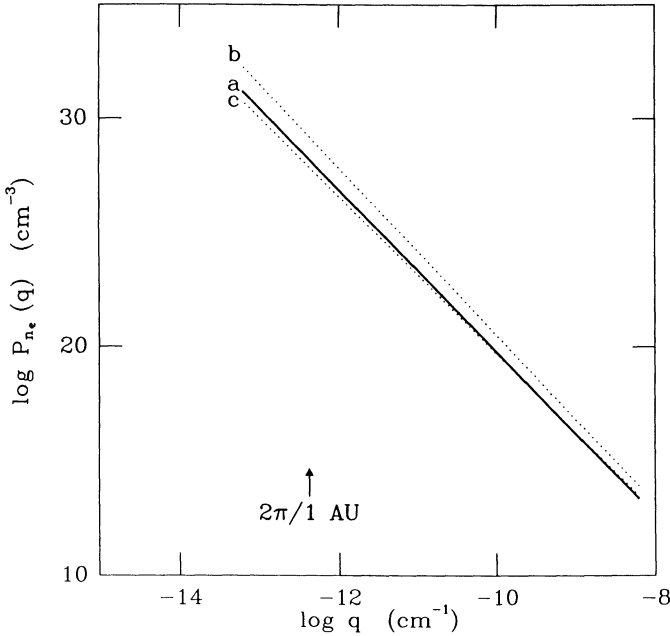


FIG. 14.—Schematic spectrum showing constraints on the electron density wavenumber spectrum along the line of sight to 1937+214. The plotted lines extend to wavenumbers corresponding to length scales between 10^{14} and 10^9 cm and could extend much further to both larger and smaller wavenumbers. (a) The spectrum using $\alpha = 3.55$ and the nominal distance of 5 kpc in eq. (9); (b) the spectrum for $\alpha = 3.66$ and a distance of 2 kpc. This lower distance is consistent with the dispersion measure and a mean electron density of 0.028 cm^{-3} ; and (c) the spectrum for $\alpha = 3.44$ and the nominal distance of 5 kpc.

wavenumber components implied by ionized regions of parsec size. Figure 14 applies to a single line of sight and is based on more precise measurements than was the spectrum of Armstrong *et al.* The spectrum appears to cover three, or, more likely, at least five orders of magnitude in wavenumber.

The spectrum may be integrated over wavenumber to yield the rms electron density for the scattering and refracting medium. Integrating equation (8) subject to the outer scale being much larger than the inner scale ($l_0 \gg l_1$), we find

$$\langle n_e^2 \rangle \approx \frac{4\pi C_n^2}{\alpha - 3} \left(\frac{l_0}{2\pi} \right)^{\alpha - 3}.$$

Since we have found that $\alpha \approx 3.55$, $l_0 \geq 10^{14}$ cm, and $C_n^2 \approx 10^{-3} \text{ m}^{-20/3}$, the rms electron density is

$$\langle n_e^2 \rangle^{1/2} \approx 10^{-3.5} \text{ cm}^{-3} \left(\frac{l_0}{10^{14}} \right)^{0.55}.$$

This rms density is about 1% of the mean (line-of-sight averaged) electron density found toward pulsars, $n_e \approx 0.03$

cm^{-3} (e.g., Weisberg, Rankin, and Boriakoff 1980). An outer scale of 0.1 pc would bring the rms equal to the mean.

VI. SUMMARY AND CONCLUSIONS

In this paper we have shown the following:

1. The narrow pulse and small period of PSR 1937+214 yield arrival times that are much more precise than those of most other pulsars.

2. Arrival time precision for 1937+214 is limited at low frequencies by distortions of the pulse shape imposed by interstellar scintillations. On short time scales (minutes), these distortions are caused by nonconvergent changes in frequency structure across the receiver bandwidth. On time scales of months or longer, pulse shape distortions are caused by variable refraction in the interstellar medium.

3. Arrival times at all radio frequencies are affected by variations in dispersion measure $\delta\text{DM} \approx 0.003 \text{ pc cm}^{-3}$ over 1000 days and, possibly, additional variations related to variations in angle of arrival.

4. Uncertainties in how the pulse shape varies with frequency influence estimates of dispersion measures. Shape variations and the precision to which DM-induced timing perturbations can be removed from arrival times will have a large influence on the implied precision of PSR 1937+214 as a clock.

5. The interstellar scintillations and pulse broadening of 1937+214 strongly constrain the spatial power spectrum of electron density variations in the interstellar medium. From the scaling of measured (diffractive scintillation) parameters with frequency and from the time variations of the parameters, we deduce that the power spectrum is consistent with the form (wavenumber) $^{-\alpha}$, where $\alpha \approx 3.55 \pm 0.11$. The diffraction pattern has a length scale at 0.43 GHz $l_d \approx \Delta t_d V_{\text{ISS}} \approx 10^9$ cm. Irregularities in the interstellar medium cover a broad range, with some of them smaller than the Fresnel scale $l_F \approx (\lambda D/2)^{1/2} \approx 10^{11.9}$ cm and some smaller than the diffraction scale l_d . The frequency-drifting phenomenon, due to refraction from structures larger than those that dominate the diffraction, implies the presence of irregularities at least as large as the refraction scale (cf. § V f), $l_R \approx l_F^2/l_d \approx 10^{14.3}$ cm (13 AU). Thus the wavenumber spectrum appears to cover at least $l_r/l_d \approx 5$ decades in scale size.

We thank Don Backer, Carl Gwinn, Roger Foster, Lloyd Rawley, Steve Spangler, Joe Taylor, and Joel Weisberg for useful conversations and Lloyd Rawley for use of his unpublished scintillation data. This research was supported by NSF grant 85-20530 to Cornell University, by the Alfred P. Sloan Foundation, and by the National Astronomy and Ionosphere Center at Cornell University, which operates the Arecibo Observatory under contract with the National Science Foundation.

APPENDIX

PULSE BROADENING AND SCINTILLATION BANDWIDTH MEASUREMENTS

Temporal broadening of pulses and scintillation frequency structure are different aspects of the same phenomenon, namely path length differences caused by scattering in the interstellar medium. The broadening time τ_d and scintillation bandwidth $\Delta\nu_d$ satisfy an uncertainty relation $2\pi\tau_d\Delta\nu_d \equiv K_1 \approx 1$ (Backer 1974; Slee, Dulk, and Otrupcek 1982) and since $\Delta\nu_d \propto \nu^{4.4}$ (CWB), it is easiest to measure τ_d at low frequencies where it is larger than the intrinsic pulse width and $\Delta\nu_d$ at high frequencies, where it is easily resolved with available spectrometers.

Temporal broadening estimation involves a minimum of data analysis: deconvolution of an assumed intrinsic pulse shape from the measured one. Estimating the intrinsic pulse shape provides the largest source of error, as we found in § IIIc. By contrast, scintillation bandwidth measurements involve a large amount of data processing, but they are generally *insensitive* to the intrinsic pulse shape. This may be seen as follows.

After passing through the antenna and receiver system, the pulsar signal conforms to the amplitude modulated noise model (Rickett 1975), in which the complex, narrow-band (scalar) electric field after mixing to base band (see text) is

$$\epsilon_p(t) = [a(t)m(t) + n(t)] * b(t), \quad (\text{A1})$$

where the asterisk denotes convolution and $b(t)$ is the Fourier transform of the receiver frequency response; $n(t)$ and $m(t)$ are complex Gaussian random processes, the former associated with additive sky and receiver noise, the latter with the emission process in the pulsar. Accordingly, they are statistically independent. Each is correlated only over a time equal to the reciprocal receiver bandwidth, or 4–8 μs for data described in this paper. The real quantity $a(t)$ models individual pulse features and is therefore correlated over much longer times than are n or m .

Modifications of the signal by propagation through the ISM are not included in equation (A1). Dispersion rotates phases of the Fourier components of ϵ_p and can be removed by correcting the phases, as we have done with our data (see main text). Scattering is modeled by multiplying the Fourier transform of $a(t)m(t)$ by a complex quantity $\tilde{s}(v)$, the squared magnitude of which is the *instantaneous* spectral modulation (over the receiver bandpass) of the pulsar signal caused by multipath scattering. In the time domain, scattering appears as a convolution by a complex function, $s(t)$. Upon taking the squared magnitude of the modified signal and taking an ensemble average (assumed equivalent to averaging over an infinite number of pulses), one obtains for the average pulse shape

$$I(t) = N(t) + A(t) * S(t) * B(t), \quad (\text{A2})$$

where $N(t) \equiv \langle |n(t)|^2 \rangle$, $A(t) = \langle a(t)^2 \rangle$, $S(t) = \langle s(t)^2 \rangle$, and $B(t) = \langle b(t)^2 \rangle$ and we let $\langle |m(t)|^2 \rangle = 1$. The pulse-broadening function $S(t)$ is the Fourier transform of the autocorrelation function of $\tilde{s}(v)$ (e.g., Rickett 1977). In practice $B(t)$ is a pulselike function much narrower than $A(t)$, so equation (A2) expresses the well-known result that the scattering acts as a linear filter that broadens the intrinsic pulse shape according to the broadening function $S(t)$.

For the regime where the integration time is less than the characteristic scintillation time, but includes a large number of pulses, equation (A2) still holds, except that $S(t)$ then does not represent an ensemble average of the scintillations. Rather, it is the “instantaneous” pulse-broadening function determined by the autocorrelation of the particular *realization* of frequency structure in the receiver bandpass. For bandwidths not much larger than the scintillation bandwidth, the instantaneous broadening function can deviate significantly from its average, thus inducing shape variations of $I(t)$. Shape variations, in turn, result in errors in estimates of time of arrival.

Frequency structure in the spectrum is usually studied after integrating over a large number of pulses. The ensemble average of the squared magnitude of the Fourier transform may be written as

$$\tilde{I}(v) = \tilde{B}(v)[\tilde{N}(v) + \text{constant} \times \tilde{S}(v)]. \quad (\text{A3})$$

The constant in equation (A3) involves an integral over frequency of the ensemble average of $|a(v)|^2$. For single realizations of data, frequency structure associated with the intrinsic pulse shape would appear as 100% modulations in a spectrum formed using the squared magnitude of a single Fourier transform of data (Rickett 1975; Cordes and Hankins 1979), even if the data interval is many pulse periods. In practice, we Fourier transform the complex signal ϵ_p , take the squared magnitude, and incoherently average over a time T that is many pulse periods but is smaller than the scintillation time $\Delta t_d \approx 100$ s at 430 MHz, over which the quantity $s(t)$ and, hence, $S(v)$ may be assumed constant. This averaging time is sufficient to wash out contributions to the frequency structure from the intrinsic pulse shape. In our data analysis, we have summed over 100 blocks of data to form each spectrum, so intrinsic fluctuations diminish to only 10% in the spectrum and 1% in the autocorrelation analysis.

From equation (A3), it is easy to see that calibration of the spectrum, i.e., division by the known receiver bandpass shape $B(v)$ and subtraction of system noise $N(v)$, yields the scintillation spectrum $\langle \tilde{S}(v) \rangle$. Statistical analysis of the scintillation spectrum, as described in the text, yields the characteristic scintillation bandwidth at each epoch.

REFERENCES

- Alpar, M. A., Nandkumar, R., and Pines, D. 1986, *Ap. J.*, **311**, 197.
 Alurkar, S. K., Slee, O. B., and Bobra, A. D. 1986, *Australian J. Phys.*, **39**, 433.
 Armstrong, J. W. 1984, *Nature*, **307**, 527.
 Armstrong, J. W., Cordes, J. M., and Rickett, B. J. 1981, *Nature*, **291**, 561.
 Backer, D. C. 1973, *Ap. J.*, **182**, 245.
 ———. 1974, *Ap. J.*, **190**, 667.
 ———. 1986, personal communication.
 Barnard, J., and Arons, J. 1986, *Ap. J.*, **302**, 138.
 Blandford, R. D., Narayan, R., and Romani, R. 1984, *J. Ap. Astr.*, **5**, 369.
 Boriakoff, V. 1973, Ph.D. thesis, Cornell University.
 Boynton, P. E., et al. 1972, *Ap. J.*, **175**, 217.
 Coles, W. A., Frehlich, R. G., Rickett, B. J., and Codona, J. L. 1987, *Ap. J.*, **315**, 666.
 Cordes, J. M. 1978, *Ap. J.*, **222**, 1006.
 ———. 1981, in *Pulsars*, ed. W. Sieber and R. Wielebinski (Dordrecht: Reidel), p. 115.
 ———. 1986, *Ap. J.*, **311**, 183.
 Cordes, J. M., and Downs, G. S. 1985, *Ap. J. Suppl.*, **59**, 343.
 Cordes, J. M., and Hankins, T. H. 1979, *Ap. J.*, **233**, 981.
 Cordes, J. M., and Helfand, D. J. 1980, *Ap. J.*, **239**, 640.
 Cordes, J. M., Pidwerbetsky, A., and Lovelace, R. V. E. L. 1986, *Ap. J.*, **310**, 737 (CPL).
 Cordes, J. M., and Stinebring, D. R. 1984, *Ap. J. (Letters)*, **277**, L53.
 Cordes, J. M., Weisberg, J. M., and Boriakoff, V. 1985, *Ap. J.*, **288**, 221 (CWB).
 Davis, M. M., Taylor, J. H., Weisberg, J. M., and Backer, D. C. 1985, *Nature*, **315**, 547.
 Dennison, B., Thomas, M., Booth, R. S., Brown, R. L., Broderick, J. J., and Condon, J. J. 1984, *Astr. Ap.*, **135**, 199.
 Downs, G. S., and Krause-Polstorff 1986, *Ap. J. Suppl.*, **62**, 81.
 Downs, G. S., and Reichley, P. E. 1983, *Ap. J. Suppl.*, **53**, 169.
 Goodman, J., and Narayan, R. 1985, *M.N.R.A.S.*, **214**, 519.
 ———. 1989, *M.N.R.A.S.*, **238**, 995.
 Gwinn, C. R., Moran, J. M., and Reid, M. J. 1988, in *Radio Wave Scattering in the Interstellar Medium* (AIP Conf. Proc. 174), ed. J. M. Cordes, B. J. Rickett, and D. C. Backer (New York: AIP), p. 129.
 Hankins, T. H. 1971, *Ap. J.*, **169**, 487.

- Hankins, T. H., and Rickett, B. J. 1975, *Meth. Comp. Phys.*, **14**, 55.
 ———. 1986, *Ap. J.*, **311**, 684.
 Heiles, C., Kulkarni, S. R., Stevens, M. A., Backer, D. C., and Davis, M. M. 1983, *Ap. J. (Letters)*, **273**, L75.
 Helfand, D. J., Manchester, R. N., and Taylor, J. H. 1975, *Ap. J.*, **198**, 661.
 Helfand, D. J., Taylor, J. H., Backus, P. R., and Cordes, J. M. 1980, *Ap. J.*, **237**, 206.
 Hewish, A. 1980, *M.N.R.A.S.*, **192**, 799.
 Kapoor, R. C., and Datta, B. 1986, *Ap. J.*, **311**, 680.
 Krishnamohan, S., and Downs, G. S. 1983, *Ap. J.*, **265**, 372.
 Lee, L. C., and Jokipii, J. R. 1976, *Ap. J.*, **206**, 735.
 Lovelace, R. V. E. 1970, Ph.D. thesis, Cornell University.
 Lyne, A. G., and Manchester, R. N. 1988, *M.N.R.A.S.*, **234**, 477.
 Manchester, R. N., and Taylor, J. H. 1981, *A.J.*, **86**, 1953.
 Manchester, R. N., Taylor, J. H., and Van, Y. 1974, *Ap. J. (Letters)*, **189**, L119.
 Matese, J. J., and Whitmire, D. P. 1980, *Ap. J.*, **235**, 587.
 Melrose, D. B. 1979, *Australian J. Phys.*, **32**, 61.
 Narayan, R. 1988, in *Radio Wave Scattering in the Interstellar Medium* (AIP Conf. Proc. 174), ed. J. M. Cordes, B. J. Rickett, and D. C. Backer (New York: AIP), p. 17.
 Pidworbetsky, A. 1988, Ph.D. thesis, Cornell University.
 Rankin, J. M. 1983, *Ap. J.*, **274**, 333.
 Rawley, L. A. 1986, Ph.D. thesis, Princeton University.
 Rawley, L. A., Taylor, J. H., and Davis, M. M. 1988, *Ap. J.*, **326**, 947.
 Rawley, L. A., Taylor, J. H., Davis, M. M., and Allan, D. W. 1987, *Science*, **238**, 761.
 Rickett, B. J. 1975, *Ap. J.*, **197**, 185.
 ———. 1977, *Ann. Rev. Astr. Ap.*, **15**, 479.
 Rickett, B. J. 1988, in *Radio Wave Scattering in the Interstellar Medium* (AIP Conf. Proc. 174), ed. J. M. Cordes, B. J. Rickett, and D. C. Backer (New York: AIP), p. 2.
 Rickett, B. J., Coles, W. A., and Bourgois, G. 1984, *Astr. Ap.*, **134**, 390.
 Romani, R. W., Narayan, R., and Blandford, R. D. 1986, *M.N.R.A.S.*, **220**, 19.
 Shishov, V. I. 1974, *Soviet Astr.*, **17**, 598.
 Shitov, Y. 1984, *Soviet Astr.*, **27**, 315.
 Simonetti, J. H., Cordes, J. M., and Heesch, D. 1986, *Ap. J.*, **296**, 46.
 Slee, O. B., Dulk, G. A., and Otrupcek, R. E. 1980, *Proc. Astr. Soc. Australia*, **4**, 100.
 Spangler, S. R., and Cordes, J. M. 1988, in *Radio Wave Scattering in the Interstellar Medium* (AIP Conf. Proc. 174), ed. J. M. Cordes, B. J. Rickett, and D. C. Backer (New York: AIP), p. 117.
 Spangler, S. R., Fey, A. L., and Cordes, J. M. 1987, *Ap. J.*, **322**, 909.
 Stinebring, D. R. 1983, *Nature*, **302**, 690.
 Stinebring, D. R., Boriakoff, V., Wolszczan, A., and Cordes, J. M. 1984, in *Millisecond Pulsars*, ed. D. Stinebring and S. Reynolds (Green Bank: NRAO), p. 32.
 Stinebring, D. R., and Condon, J. J. 1990, *Ap. J.* submitted.
 Stinebring, D. R., and Cordes, J. M. 1983, *Nature*, **306**, 349.
 Taylor, J. H., and Huguenin, G. R. 1971, *Ap. J.*, **167**, 273.
 Weisberg, J. M., Rankin, J. M., and Boriakoff, V. 1980, *Astr. Ap.*, **88**, 84.
 Wilkinson, P. N., Spencer, R. E., and Nelson, R. F. 1988, in *IAU Symposium 129, The Impact of VLBI on Astrophysics and Geophysics*, ed. M. J. Reid and J. M. Moran (Dordrecht: Reidel), p. 305.
 Williamson, I. P. 1972, *M.N.R.A.S.*, **157**, 55.
 ———. 1975, *Proc. Roy. Soc. London A*, **342**, 131.

MICHAEL BLASKIEWICZ and JAMES M. CORDES: Astronomy Department, Space Sciences Building, Cornell University, Ithaca, NY 14853

RACHEL J. DEWEY: Jet Propulsion Laboratory, California Institute of Technology, Oak Grove Drive, Pasadena, CA 91109

DANIEL R. STINEBRING: Department of Physics, Princeton University, Princeton, NJ 08544

ALEXANDER WOLSZCZAN: Arecibo Observatory, P.O. Box 995, Arecibo, PR 00613